NASA/CR-1999-209555

Transonic Dynamics Tunnel Force and Pressure Data Acquired on the HSR Rigid Semispan Model

David M. Schuster and Russ D. Rausch
Lockheed Martin Engineering and Sciences Company, Hampton, Virginia

September 1999

The NASA STI Program Office . . . in Profile

Since its founding, NASA has been dedicated to the advancement of aeronautics and space science. The NASA Scientific and Technical Information (STI) Program Office plays a key part in helping NASA maintain this important role.

The NASA STI Program Office is operated by Langley Research Center, the lead center for NASA's scientific and technical information. The NASA STI Program Office provides access to the NASA STI Database, the largest collection of aeronautical and space science STI in the world. The Program Office is also NASA's institutional mechanism for disseminating the results of its research and development activities. These results are published by NASA in the NASA STI Report Series, which includes the following report types:

- TECHNICAL PUBLICATION. Reports of completed research or a major significant phase of research that present the results of NASA programs and include extensive data or theoretical analysis. Includes compilations of significant scientific and technical data and information deemed to be of continuing reference value. NASA counterpart or peer-reviewed formal professional papers, but having less stringent limitations on manuscript length and extent of graphic presentations.

- TECHNICAL MEMORANDUM. Scientific and technical findings that are preliminary or of specialized interest, e.g., quick release reports, working papers, and bibliographies that contain minimal annotation. Does not contain extensive analysis.

- CONTRACTOR REPORT. Scientific and technical findings by NASA-sponsored contractors and grantees.

- CONFERENCE PUBLICATION. Collected papers from scientific and technical conferences, symposia, seminars, or other meetings sponsored or co-sponsored by NASA.

- SPECIAL PUBLICATION. Scientific, technical, or historical information from NASA programs, projects, and missions, often concerned with subjects having substantial public interest.

- TECHNICAL TRANSLATION. English-language translations of foreign scientific and technical material pertinent to NASA's mission.

Specialized services that complement the STI Program Office's diverse offerings include creating custom thesauri, building customized databases, organizing and publishing research results . . . even providing videos.

For more information about the NASA STI Program Office, see the following:

- Access the NASA STI Program Home Page at *http://www.sti.nasa.gov*

- Email your question via the Internet to help@sti.nasa.gov

- Fax your question to the NASA STI Help Desk at (301) 621-0134

- Telephone the NASA STI Help Desk at (301) 621-0390

- Write to:
  NASA STI Help Desk
  NASA Center for AeroSpace Information
  7121 Standard Drive
  Hanover, MD 21076-1320

NASA/CR-1999-209555

Transonic Dynamics Tunnel Force and Pressure Data Acquired on the HSR Rigid Semispan Model

David M. Schuster and Russ D. Rausch
Lockheed Martin Engineering and Sciences Company, Hampton, Virginia

National Aeronautics and
Space Administration

Langley Research Center
Hampton, Virginia 23681-2199

Prepared for Langley Research Center
under Contract NAS1-96014

September 1999

The use of trademarks or names of manufacturers in this report is for accurate reporting and does not constitute an official endorsement, either expressed or implied, of such products or manufacturers by the National Aeronautics and Space Administration.

Available from:

NASA Center for AeroSpace Information (CASI)
7121 Standard Drive
Hanover, MD 21076-1320
(301) 621-0390

National Technical Information Service (NTIS)
5285 Port Royal Road
Springfield, VA 22161-2171
(703) 605-6000

Introduction

This report describes the aerodynamic data acquired on the High Speed Research Rigid Semispan Model (HSR-RSM) during NASA Langley Transonic Dynamics Tunnel (TDT) Test 520 conducted from 18 March to 4 April, 1996. The purpose of this test was to assess the aerodynamic character of a rigid high speed civil transport wing. The wing was fitted with a single trailing edge control surface which was both steadily deflected and oscillated during the test to investigate the response of the aerodynamic data to steady and unsteady control motion. Angle-of-attack and control surface deflection polars at subsonic, transonic and low-supersonic Mach numbers were obtained in the tunnel's heavy gas configuration.

Unsteady pressure and steady loads data were acquired on the wing, while steady pressures were measured on the fuselage. These data were reduced using a variety of methods, programs and computer systems. The reduced data was ultimately compiled onto a CD-ROM volume which was distributed to HSR industry team members in July, 1996. This report documents the methods used to acquire and reduce the data, and provides an assessment of the quality, repeatability, and overall character of the aerodynamic data measured during this test.

Model Description

Wing Model and Instrumentation

The HSR-RSM wing is a modified 1/12 scale model of the Boeing Reference HSCT Configuration (Reference H). The HSR-RSM wing planform is shown in Figure 1 Modifications to the basic Reference H configuration include removal of the inboard trailing edge extension, and the scaling of the airfoil sections so that a constant 4% thick section is maintained over the entire wing planform. The thickness scaling was performed so as to provide sufficient outboard wing volume for the pressure, accelerometer and strain gauge instrumentation. The trailing edge flap employed on the HSR-RSM is not designed to be representative of control systems to be used on HSCT flight vehicles, but rather as a mechanical artifice for exciting the flowfield about the wing for unsteady aerodynamic observations. A pair of flow-through nacelles were also fabricated to determine the impact of these components on the aerodynamics of the wing. As shown in the figure, the nacelles are attached to short pylons along the lower surface inboard trailing edge of the wing.

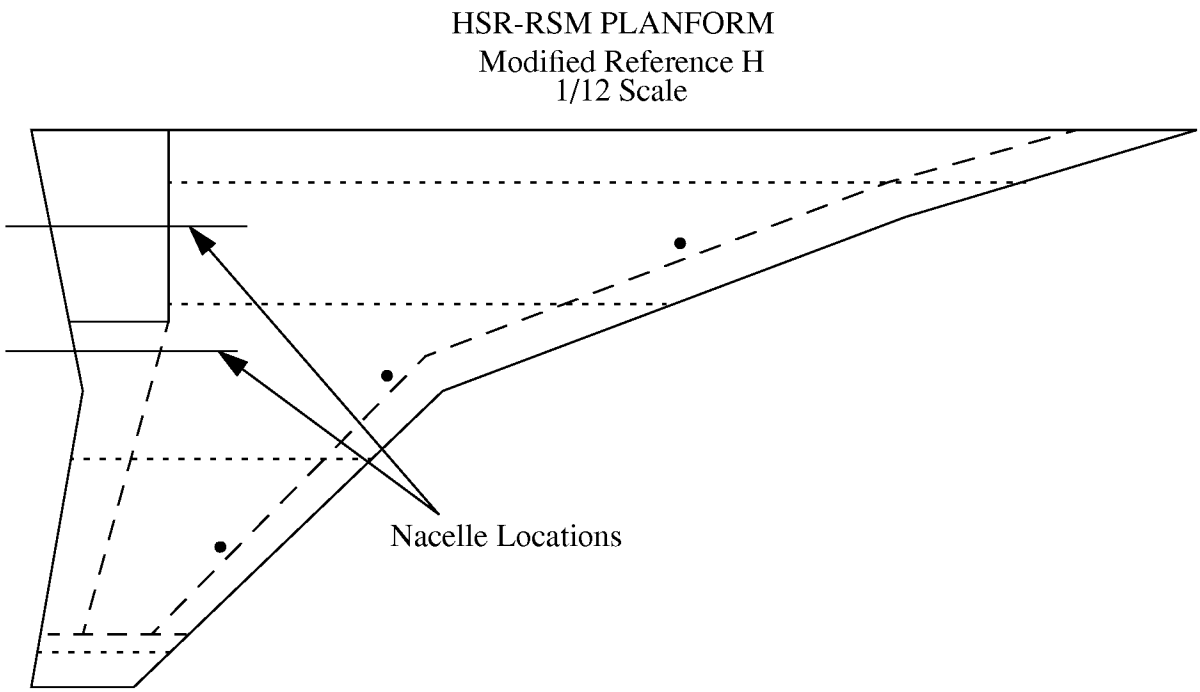

Figure 1. HSR Rigid Semispan Model Wing Planform.

The wing is primarily of carbon graphite composite and foam construction. It consists of five major components, the main wing box, leading and trailing edge fairings, a wing tip cap and instrumentation holder, and the trailing edge flap. The largest section of the wing, the wing box, consists of a two-piece foam core bonded to carbon graphite external skins. The dashed lines in Figure 1 represent seams between the main wing box and the removable leading edge, trailing edge and wing tip sections. These fairings provide access to instrumentation in these areas and also serve as routing paths for wiring and pressure reference tubes. Instrumentation is also routed through conduit in the main wing foam core.

The chordwise dotted lines in Figure 1 represent the locations of the primary pressure instrumentation on the wing. Pressure transducers are located at 10, 30, 60 and 95 percent span. There are a total of 137 wing pressure transducers. As shown in the figure, the 10 and 30 percent span locations contain pressure instrumentation only as far back as the leading edge of the flap. The 60 and 95 percent span locations contain instrumentation all of the way to the wing trailing edge. Table 1 lists the fractional chordwise location of each pressure transducer at these four span stations. In addition to these 131 pressures there are six pressures located on the upper and lower surfaces at 20 percent chord and 20, 45 and 75 percent span, shown by the solid circles in the figure.

The wing is mounted on a five-component force balance located at the wing root. The balance measures normal and axial loads along with pitch, yaw and roll moments. The fuselage is mounted so that it does not transfer load to the balance, thus in the test configuration described in this report, only wing loads are monitored by the balance.

Table 1. Wing surface pressure transducer locations

Upper Surface							
10% Span		30% Span		60% Span		95% Span	
X/C	Channel Number	X/C	Channel Number	X/C	Channel Number	X/C	Channel Number
0.0	151	0.0	111	0.0	65	0.0	31
0.025	186	0.025	145	0.05	66	0.10	32
0.05	152	0.05	112	0.10	67	0.20	33
0.10	153	0.10	113	0.15	68	0.30	34
0.15	154	0.15	114	0.20	69	0.40	35
0.20	155	0.20	115	0.25	70	0.50	36
0.25	156	0.25	116	0.30	71	0.60	37
0.30	157	0.30	117	0.35	72	0.70	38
0.35	158	0.35	118	0.40	73	0.80	39
0.40	159	0.40	119	0.45	74	0.90	40
0.45	160	0.45	120	0.50	75		
0.50	161	0.50	121	0.55	76		
0.55	162	0.55	122	0.60	77		
0.60	163	0.60	123	0.65	78		
0.65	164	0.65	124	0.70	79		
0.70	165	0.70	125	0.75	80		
0.75	166	0.75	126	0.80	81		
0.80	167	0.80	127	0.85	82		
0.85	168			0.90	83		
				0.95	84		
				1.0	85		

Table 1. Wing surface pressure transducer locations

Lower Surface							
10% Span		30% Span		60% Span		95% Span	
X/C	Channel Number	X/C	Channel Number	X/C	Channel Number	X/C	Channel Number
0.025	187	0.025	146	0.05	86	0.10	42
0.05	169	0.050	129	0.10	87	0.20	43
0.10	170	0.10	130	0.15	88	0.30	44
0.15	171	0.15	131	0.20	89	0.40	45
0.20	172	0.20	132	0.25	90	0.50	46
0.25	173	0.25	133	0.30	91	0.60	47
0.30	174	0.30	134	0.35	92	0.70	48
0.35	175	0.35	135	0.40	93	0.80	49
0.40	176	0.40	136	0.45	94	0.90	50
0.45	177	0.45	137	0.50	95		
0.50	178	0.50	138	0.55	96		
0.55	179	0.55	139	0.60	97		
0.60	180	0.6	140	0.65	98		
0.65	181	0.65	141	0.70	99		
0.70	182	0.70	142	0.75	100		
0.75	183	0.75	143	0.80	101		
0.80	184	0.80	144	0.85	102		
0.85	185			0.90	103		
				0.95	104		

Fuselage Model and Instrumentation

A schematic of the HSR-RSM fuselage is shown in Figure 2. The fuselage serves primarily as a fairing for the wing mounting hardware, instrumentation wiring, and pressure reference tubes. It also serves as a spacer to displace the wing away from the wind tunnel wall and out of its boundary layer. However, since it is in close proximity to the wing, it provides aerodynamic interference which must be accounted for in theoretical models. Therefore, it is also equipped with pressure measurement instrumentation. Steady pressure measurements are made at seven stations along the fuselage. Pressure ports are spaced in the circumferential direction at each constant fuselage station. In total, there are 119 ports on the fuselage surface. The location and corresponding data channel number for each of these ports is presented in Table 2.

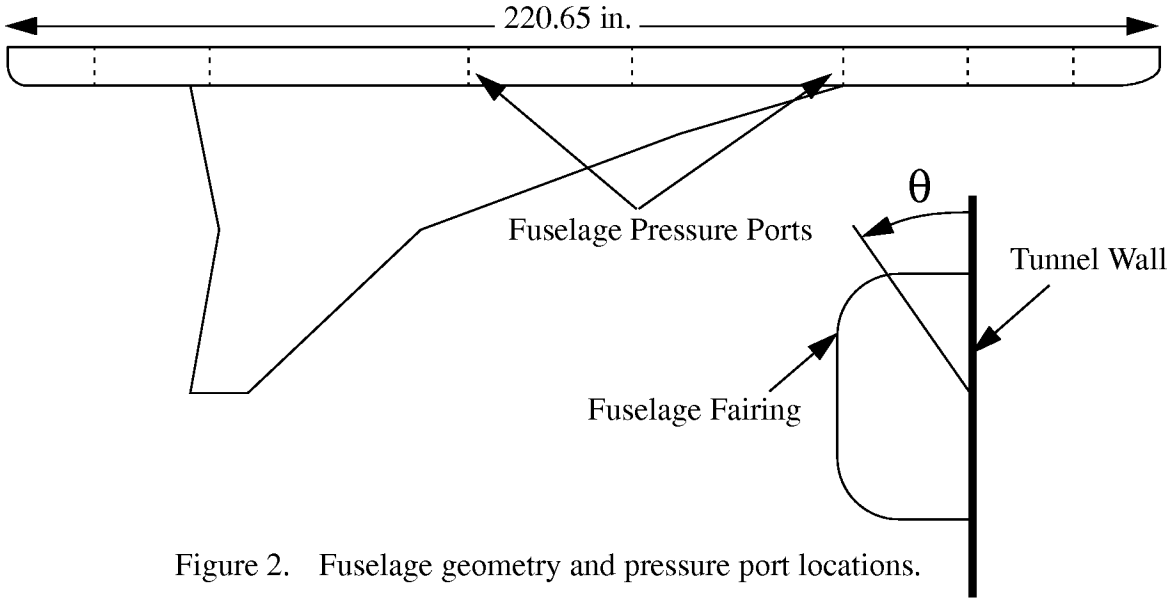

Figure 2. Fuselage geometry and pressure port locations.

Table 2. HSR-RSM fuselage pressure port locations

Fuselage Pressure Port Locations θ measured from upper fuselage symmetry plane							
X = 16 in.		X = 36 in.		X = 60 in.		X = 102 in.	
θ (°)	Channel	θ (°)	Channel	θ (°)	Channel	θ (°)	Channel
9.23	1	7.97	17	7.97	33	54.00	49
13.78	2	15.64	18	15.64	34	57.13	50
18.22	3	22.78	19	22.78	35	60.23	51
26.56	4	35.26	20	35.26	36	63.30	52
40.71	5	54.00	21	54.00	37	66.36	53
47.33	6	66.36	22	66.36	38	67.93	54
80.99	7	79.81	23	79.81	39	69.53	55
90.00	8	90.00	24	90.00	40	71.17	56
99.01	9	100.19	25	100.19	41	108.83	57
132.67	10	113.64	26	113.64	42	110.47	58
139.29	11	126.00	27	126.00	43	112.07	59
153.44	12	144.74	28	144.74	44	113.64	60
161.78	13	157.22	29	157.22	45	119.77	61
166.22	14	164.36	30	164.36	46	122.87	62
170.77	15	172.03	31	172.03	47	126.00	63

Table 2. HSR-RSM fuselage pressure port locations

Fuselage Pressure Port Locations θ measured from upper fuselage symmetry plane							
X = 132 in. (Upper)		X =132 in. (Lower)		X = 182 in.		X = 204 in.	
θ (°)	Channel	θ (°)	Channel	θ (°)	Channel	θ (°)	Channel
7.97	65	107.16	81	7.97	97	7.97	113
15.64	66	108.83	82	15.64	98	15.64	114
22.78	67	110.47	83	22.78	99	22.78	115
29.24	68	112.07	84	35.26	100	35.26	116
35.26	69	113.64	85	54.00	101	54.00	117
41.43	70	116.70	86	66.36	102	66.36	118
54.00	71	119.77	87	79.81	103	79.81	119
57.13	72	122.87	88	90.00	104	90.00	120
60.23	73	126.00	89	100.19	105	100.19	121
63.30	74	138.57	90	113.64	106	113.64	122
66.36	75	144.74	91	126.00	107	126.00	123
67.93	76	150.76	92	144.74	108	144.74	124
69.53	77	157.22	93	157.22	109	157.22	125
71.17	78	164.36	94	164.36	110	164.36	126
		172.03	95	172.03	111	172.03	127

Test Conditions and Data Summary

The HSR-RSM was tested over a wide range of flight conditions. A series of angle-of-attack and flap deflection polars were acquired for Mach numbers ranging from 0.7 to 1.15. The model angle-of-attack was limited by the balance load limits and typically varied between -2 and 8 degrees. Flap deflections were limited to +/- 5 degrees. Freestream dynamic pressure was also varied to assess its impact on the quality of the aerodynamic data obtained and to determine if any aeroelastic effects could be observed during the testing of the model. Data at dynamic pressures of 100, 150, and 200 lbs./ft.^{2} (psf) were acquired during this test.

A summary of the angle-of-attack and flap deflection polars is presented in Table 3. In this table, the data are organized by configuration, dynamic pressure and Mach number. The run number, range of tab points and comments are provided for each variation. The major configurations tested were clean-wing and wing-with-nacelles, and clean-wing with slots open and closed. The slots refer to the slots along the wind tunnel wall on which the wing is mounted. Covers were attached to this wall to isolate it from the plenum chamber and assess the impact of these slots on the aerodynamic data.

Table 3. HSR-RSM polar summary

TDT T520 Aerodynamic Data Run Log

No Nacelles, Slots Open, AOA Polars

Mach No.	Dynamic Pressure (PSF)	Run No.	Tab Nos.	Comments
0.80	100	4	240 - 252	Possible Contaminated Data
0.80	100	6	287 -297	
0.95	100	2	160 - 172	
1.10	100	2	147 - 158	
0.98	150	4	263 - 272	Possible Contaminated Data
1.02	150	4	254 - 262	Possible Contaminated Data
1.10	150	4	229 - 239	Possible Contaminated Data

No Nacelles, Slots Closed, AOA Polars

Mach No.	Dynamic Pressure (PSF)	Run No.	Tab Nos.	Comments
0.80	100	10	463 - 479	
0.95	100	10	408 - 420	T419 Bad
0.98	100	8	364 - 376	
1.02	100	8	350 - 362	
1.05	100	8	338 - 349	
0.70	150	20	805 - 816	
0.80	150	18	729 - 742	-0.13° AOA Correction Rqd.
0.85	150	18	708 - 722	-0.13° AOA Correction Rqd.
0.90	150	12	593 - 604	
0.90	150	17	685 - 696	Repeat Run, α Tares & -0.13° AOA Correction Rqd.
0.95	150	12	574 - 585	
0.97	150	12	563 - 573	
0.98	150	12	546 - 556	
0.99	150	12	535 - 545	T535 - Missing
1.00	150	11	521 - 531	
1.02	150	11	504 - 514	T506 - Lost Weather-strip; T507 - Missing
1.05	150	11	493 - 502	
1.10	150	10	446 - 457	
1.15	150	10	433 - 444	
1.15	150	17	673 - 683	Repeat Run, α Tares & -0.13° AOA Correction Rqd.
0.80	200	20	824 - 836	
0.90	200	19	787 - 795	
0.95	200	19	774 - 781	
0.98	200	19	760 - 766	
1.02	200	19	767 - 772	
1.10	200	13	610 - 616	
1.10	200	17	697 - 704	Repeat Run, α Tares & -0.13° AOA Correction Rqd.

Table 3. HSR-RSM polar summary

TDT T520 Aerodynamic Data Run Log

No Nacelles, Slots Closed, Flap Polars

Mach No.	Dynamic Pressure (PSF)	Run No.	Tab Nos.	Comments
0.80	100	10	479 - 483	
0.95	100	10	421 - 428	
0.70	150	20	816 - 822	
0.80	150	18	742 - 747	-0.13° AOA Correction Rqd.
0.85	150	18	722 - 727	
0.95	150	12	585 - 591	
0.98	150	12	556 - 562	
1.02	150	11	514 - 520	
1.10	150	10	457 - 462	
0.80	200	20	836 - 841	
0.95	200	19	781 - 785	
0.80	100	10	487 - 489	Flap Oscillation
0.80	150	18	749 - 754	Flap Osc., -0.13° AOA Correction Rqd.

Nacelles-on, Slots Closed, AOA Polars

Mach No.	Dynamic Pressure (PSF)	Run No.	Tab Nos.	Comments
0.80	100	23	936 - 950	
0.95	100	23	916 - 929	
0.95	100	26	996 - 1009	Repeat
0.98	100	22	900 - 911	
1.02	100	22	886 - 898	
1.05	100	22	874 - 885	
1.10	100	22	863 - 873	
0.85	150	29	1170 - 1181	
0.90	150	29	1148 - 1158	
0.95	150	28	1127 - 1138	
0.97	150	28	1116 - 1126	
0.98	150	28	1102 - 1112	
0.99	150	28	1091 - 1101	
1.00	150	27 28	1075 - 1083 1087 - 1090	Tunnel Tripped Off-line
1.02	150	27	1059 - 1073	
1.05	150	27	1046 - 1058	
1.10	150	24	970 - 974	Flap Problems
1.10	150	27	1032 - 1040	
1.15	150	23	956 - 965	
1.15	150	26	1016 - 1025	Repeat
1.10	200	29	1160 - 1168	

Nacelles-on, Slots Closed, Flap Polars

Table 3. HSR-RSM polar summary

TDT T520 Aerodynamic Data Run Log

Mach No.	Dynamic Pressure (PSF)	Run No.	Tab Nos.	Comments
0.80	100	23	950 - 955	
0.95	100	23	929 - 934	
0.95	100	26	1009 - 1014	Repeat
0.85	150	29	1181 - 1185	
0.95	150	28	1138 - 1143	
0.98	150	28	1112 - 1115	
1.10	150	27	1040 - 1044	

LOADS DATA ACQUISITON AND REDUCTION

Five component aerodynamic loads data were acquired for each point at which pressure data were obtained. Side force is the only load component not measured in this test. In virtually all cases, balance limits defined the operating limits for the model. The balance limits and assumed resolution for this test are shown in Table 4. In this table, the measurement resolution was obtained by assuming the balance could resolve 1% of the component load limit. This absolute load increment was then converted to coefficient form to provide a guideline for balance resolution in terms of standard aerodynamic quantities. These resolutions are considered conservative since measurements in the TDT verified that the balance was able to resolve less than 1% of its limit load in the normal, pitch and roll components.

Table 4. Balance load limits and assumed measurement resolution

Component	Load Limit	Resolution ($\alpha = 0^o$, q = 100psf)
Normal Force	1500 lb.	ΔC_L = +/-0.00608
Axial Force	120 lb.	ΔC_D = +/-0.000487
Pitching Moment	6000 in.-lb.	ΔC_M = +/-0.000283
Rolling Moment	30,000 in.-lb.	ΔC_l = +/-0.00188
Yaw Moment	3000 in.-lb.	ΔC_n = +/-0.000188

The aerodynamic loads data presented in this report were reduced based on the diagram and reference areas and lengths presented in Figure 3. Since the planform for this model is a 1/12 scale version of the Boeing Reference H concept, the reference areas and lengths used to assess the aerodynamics of Reference H, appropriately scaled, were used for the present data reduction. The balance is located very near 50% mean aerodynamic chord, so this location was used as the

streamwise moment center. The spanwise moment center is the TDT wall, and the vertical moment center was chosen as the vertical location of the wing root leading edge. The equations used to compute the aerodynamic moments are also presented in the figure. Note that a side force coefficient is not included in the list since the balance did not measure this force component. Also, the actual equations for the moment coefficients are considerably simpler than what is shown since the side force component is zero and the streamwise location of the balance and the moment center are the same.

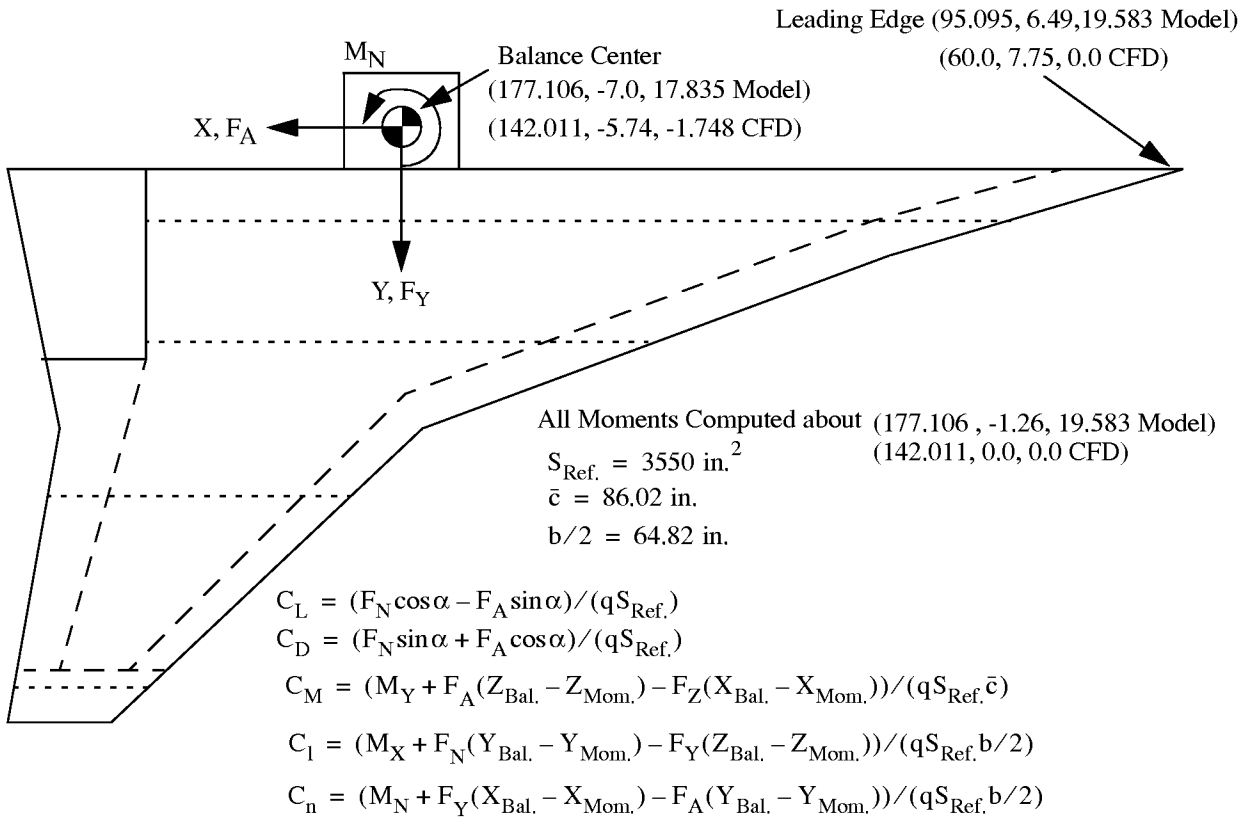

Figure 3. Reference diagram for calculation of HSR-RSM aerodynamic loads.

Before testing each configuration in the TDT, balance tares were acquired as the model angle-of-attack was varied. After the test, these tares were found to be in error. Since these tares affected only a very small portion of the data taken at each data point, the raw TDT data were not reduced a second time to correct the error. Instead, corrected alpha tares were incorporated into the data when they were post processed into the polar data presented in this report. The tares were added to the raw TDT data as a linear correction with angle-of-attack. The tare corrections used in this report are displayed in Table 5. Two sets of tares are presented here, one for the clean-wing and the other for the wing-with-nacelles.

Table 5. Angle-of-attack tares used in force data reduction.

Force Component	Angle-of-attack Tare
Clean-wing	
Normal	0.33 lb./deg.
Axial	5.33 lb./deg.
Pitch Moment	1.75 in.-lb./deg.
Roll Moment	5.10 in.-lb./deg.
Yaw Moment	66.99 in.-lb./deg.
Nacelles-on	
Normal	0.26 lb./deg.
Axial	5.60 lb./deg.
Pitch Moment	2.0 in.-lb./deg.
Roll Moment	5.41 in.-lb./deg.
Yaw Moment	75.80 in.-lb./deg.

Aerodynamic polars with respect to angle-of-attack and flap deflection were processed post test using the TDT channel statistics files generated for each tab point at which pressure data were acquired. The post processing program reads a specified set of channel statistic files, sorts them by increasing angle-of-attack or flap deflection, converts the balance data into aerodynamic coefficients based on a specified set of reference data and prints out the data in tabular form. A sample output from the force polar post processing program is shown in Figure 4. In addition to tabulating the acquired data, the post processor also curve fits the lift drag and pitching moment data using a least squares approximation. The equations used to fit the data are:

$$
\begin{aligned}
C_L &= C_{L_0} + C_{L_\alpha}\alpha \\
C_M &= C_{M_{C_L=0}} + C_{M_{C_L}} C_L \\
C_D &= C_{D_{min}} + k\left(C_L - C_{L_{C_{D_{min}}}}\right)^2
\end{aligned}
\tag{1}
$$

The lift coefficient data are fit as a function of angle-of-attack or flap deflection depending on the type of polar, and a linear approximation is used for this purpose. The coefficients C_{L_0} and C_{L_α} are the computed lift at zero AOA or flap deflection and the lift curve slope, respectively. The

pitching moment is fit as a function of lift coefficient and again a linear approximation is utilized. In this equation, $C_{M_{C_{L=0}}}$ and $C_{M_{C_L}}$ are the pitching moment at zero lift and the pitching moment slope as a function of lift coefficient, respectively. The drag coefficient fit is computed as a quadratic function of lift coefficient. The coefficient $C_{D_{min}}$ is the computed minimum drag, k is the so-called drag due to C_L^2, and $C_{L_{C_{D_{min}}}}$ is the lift coefficient at minimum drag. Each of these coefficients is computed from the least squares fit and printed with the tabular data along with the Root Mean Squared (RMS) error for each fit.

```
 T520 HSR-RSM (Balance) Force Data, Run   10
M=0.8 R12 Q=100 R10 T463-480
 ********************************************************************

Mach 0.8007   Q 101.2 psf   Re  1.880 million/ft.

 ****** Fit Data ******
CL0=-0.0510 dCL/dalpha= 0.0429         CL = CL0 + dCL/dalpha*alpha
CM0= 0.0095 dCM/dCL=-0.0585            CM = CM0 + dCM/dCL*CL
CD0= 0.0057 K= 0.3138 CLCD0= 0.0094    CD = CD0 + K*(CL-CLCD0)**2

 ****** Fit RMS Error ******
CLrms=0.00413  CMrms=0.00125  CDrms=0.00039
```

Alpha	Delf	CL	CD	CM	Cl	Cn	Tab
-2.02	-0.01	-0.1283	0.0116	0.0207	-0.0763	0.0023	467
-1.00	-0.02	-0.0924	0.0084	0.0135	-0.0521	0.0035	466
-0.03	-0.02	-0.0536	0.0068	0.0115	-0.0301	0.0039	465
0.06	-0.03	-0.0477	0.0066	0.0108	-0.0292	0.0041	468
0.99	-0.02	-0.0124	0.0060	0.0092	-0.0069	0.0041	464
1.02	-0.03	-0.0056	0.0062	0.0088	-0.0080	0.0041	470
1.02	-0.03	-0.0052	0.0061	0.0092	-0.0080	0.0041	469
1.99	-0.02	0.0279	0.0061	0.0077	0.0149	0.0041	463
1.99	-0.02	0.0279	0.0061	0.0077	0.0149	0.0041	463
2.01	-0.01	0.0288	0.0061	0.0078	0.0153	0.0039	479
2.05	-0.04	0.0384	0.0065	0.0070	0.0143	0.0038	471
3.00	-0.04	0.0792	0.0074	0.0055	0.0356	0.0032	472
4.00	-0.01	0.1160	0.0087	0.0038	0.0609	0.0032	478
4.00	-0.05	0.1220	0.0093	0.0033	0.0588	0.0028	473
5.02	-0.05	0.1683	0.0129	0.0010	0.0844	0.0027	474
6.00	-0.05	0.2100	0.0179	-0.0022	0.1079	0.0030	475
7.03	-0.05	0.2529	0.0244	-0.0065	0.1306	0.0034	476
8.01	-0.05	0.2938	0.0317	-0.0083	0.1521	0.0043	477

Figure 4. Sample tabular output from force data post processing program.

Lift drag and pitching moment data from the post processing code are also written to a separate file for plotting using the Tecplot™ graphics package. A sample force data plot is presented in Figure 5. In this figure, the experimental data points are represented by the symbols, while the curve fit data are shown by the solid line.

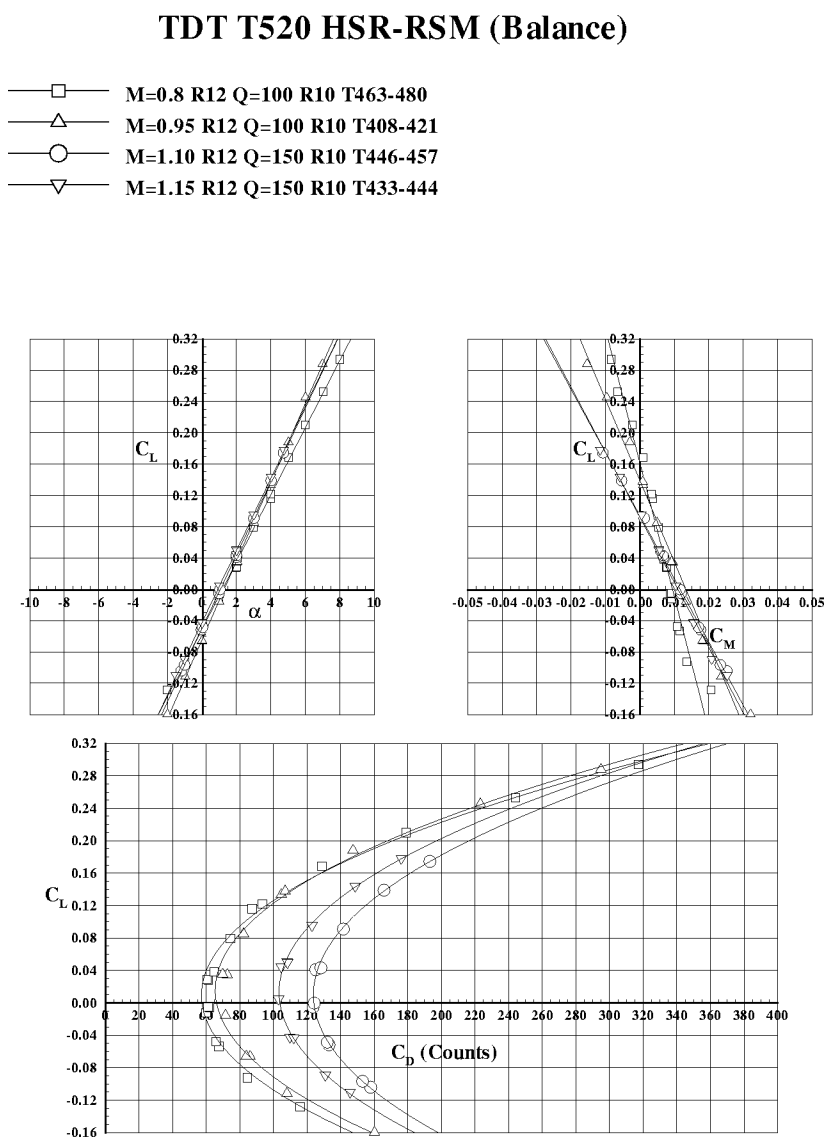

Figure 5. Sample plot from force data post processing program.

Loads Data Analysis

The tabulated loads data have been written to CD-ROM and delivered to the airframe companies along with hardcopies of the force data plots for each TDT run. Therefore, a complete listing of the tabular data and plots will not be repeated in this report. However, we will assess the character and quality of the force data by reviewing selected polars that illustrate the primary objectives of the test. We will examine the impact of closing the sidewall slots on the aerodynamic data, the variation of the data with Mach number and dynamic pressure, the effect of the nacelles, and the

performance of the control surface as a function of Mach number.

Side Wall Slot Effects

A number of semispan tests, including earlier tests of the HSR-RSM, have been conducted with all of the TDT wall slots open. These slots reduce shock reflections from the wall by allowing air to pass freely from the test section to the plenum chamber surrounding the test section. However, for semispan models this may not provide an appropriate symmetry plane boundary for the wall on which the model is mounted (TDT east wall). Preliminary CFD analyses performed at NASA Langley Research Center, McDonnell Douglas and Boeing indicated that the computed lift curve slope is considerably larger than that obtained in earlier tests of the HSR-RSM with the TDT east wall slots open. Literature also confirmed that the symmetry plane wall slots should be closed for semispan testing. Data with the east wall slots open and closed were acquired during this test of the HSR-RSM.

Figure 6 shows a comparison of the force data for the HSR-RSM wing without nacelles and with the slots open and closed for a Mach number of 0.8 and a dynamic pressure of 100psf. It is clear from the plot that closing the TDT east wall slots increases the lift curve slope. The tabulated data indicate that the lift curve slope increases by 7.5% with the slots closed. According to this plot, the pitching moment slope as a function of lift coefficient decreases, and the drag increases with the slots closed. However, the comparison of the pitching moment slopes can be misleading since both the slot-open and -closed data exhibit a significant degree of nonlinearity. The scatter in the drag data also indicates that a second order curve is probably not a good fit for these data.

Figure 7 fits the same set of data with fourth order curves for the lift and pitching moment plots and a sixth order curve for the drag. The RMS error for the lift curve is of the same order for this figure as for the previous figure, but the error for the pitching moment and drag fits are an order of magnitude smaller for the higher order fit of Figure 7. The improved nonlinear fit for the pitching moment curve shows that the wall slots have very little impact on the pitching moment data for lift coefficients between -0.06 and 0.18. Below and above these values, the slots have a significant effect. Intuitively this makes sense since as the absolute value of the angle-of-attack of the model is increased, the test section blockage increases, which will provide more opportunity for air to flow through the wall slots. The drag polar indicates that closing the wall slots effectively rotates the polar about a lift coefficient of 0.16. The drag due to lift also changes when the slots are closed.

Note that these conclusions are drawn from data at only a single flight condition. Additional slot-open data were acquired during the test, but much of these data are suspect, or do not match with slot closed data. The fact that the comparison is made at a dynamic pressure of 100 psf is also significant. It will be subsequently shown that the 100 psf dynamic pressure data do not behave as consistently as the data at higher dynamic pressures. While this comparison provides us with a gross feel for how the data behave as a function of whether the slots are open or closed, these characteristics should not be generalized at this point. Further, more detailed, testing with the slots open and closed should be performed before general conclusions can be drawn. The CFD data and literature suggest that testing with the slots closed is the proper way to proceed, and all data presented in the rest of this report is for the slots-closed configuration.

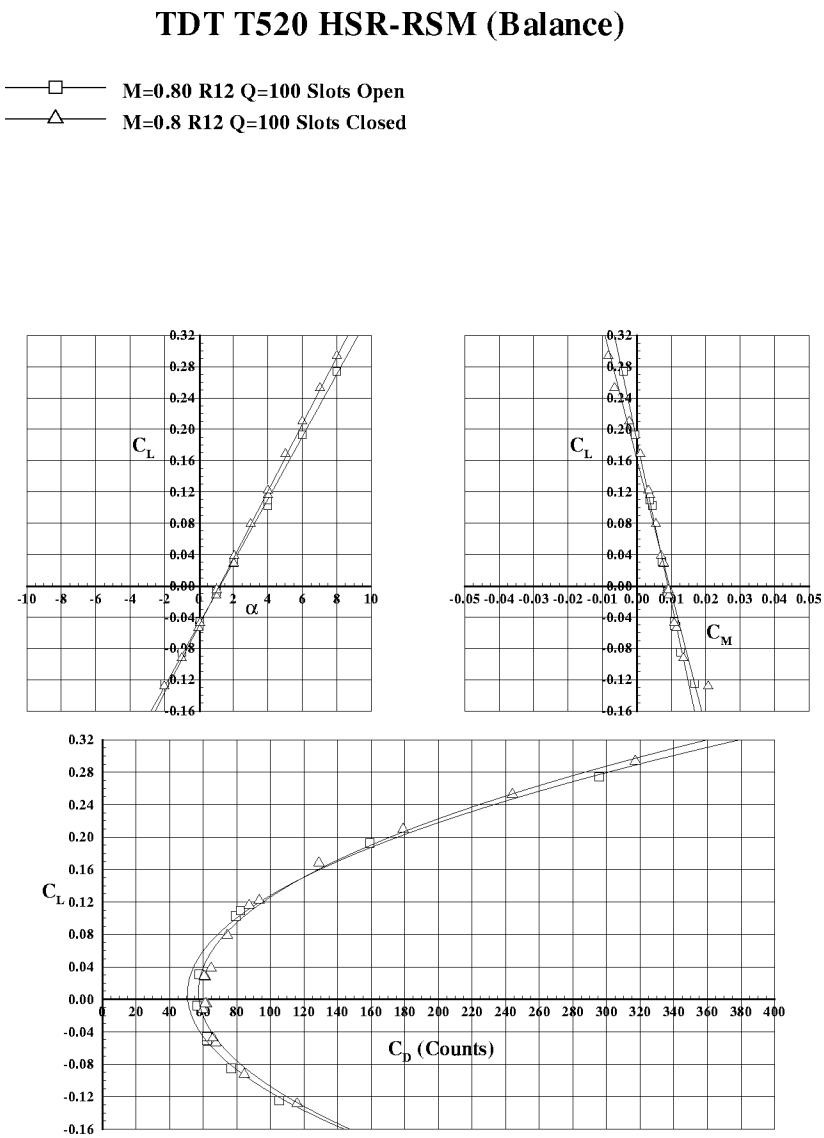

Figure 6. Comparison of loads data with TDT east wall slots open and closed.

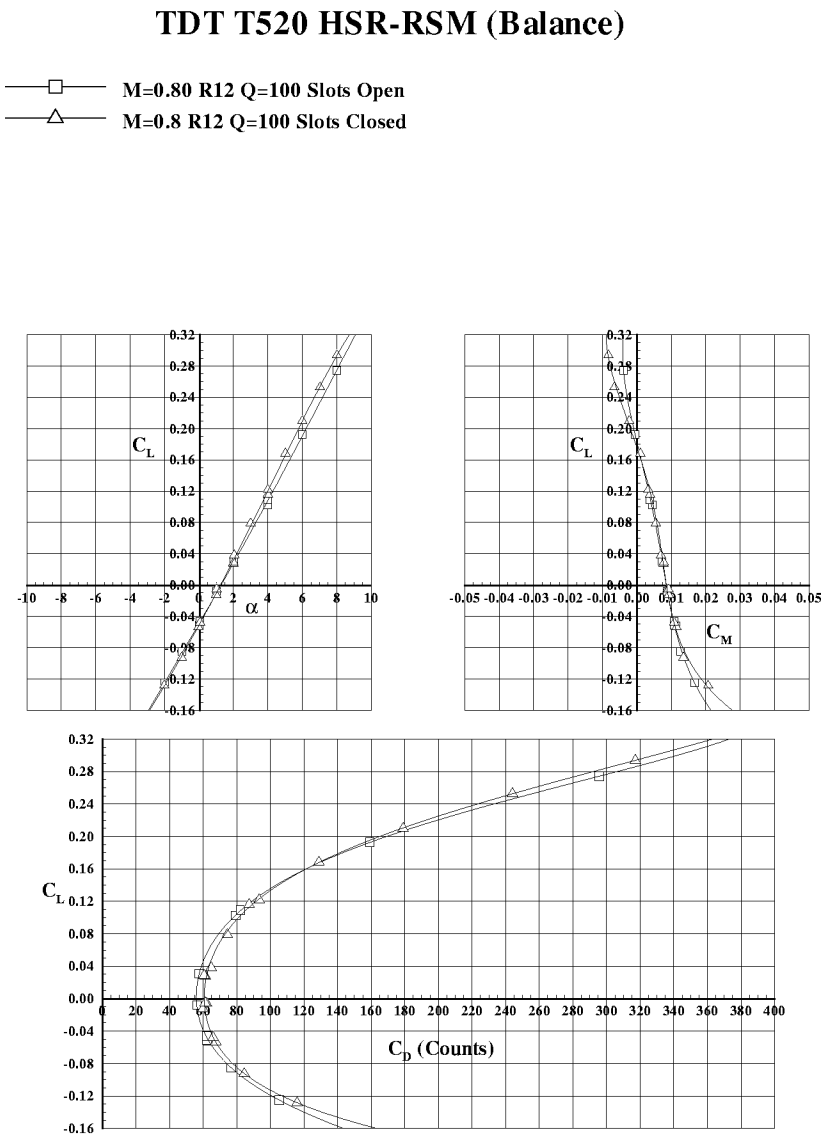

Figure 7. Higher order curve fit of slots open and closed data.

Effect of Variation of Dynamic Pressure

Dynamic pressures of 100, 150 and 200 psf were run during this test to assess the aeroelastic qualities of the model. The HSR-RSM was designed to be very stiff, and we did not expect significant aeroelastic effects due to the deformation of the model itself. However, the mounting system for the model is composed of several long slender components which may be susceptible to deflection under aerodynamic load. Figure 8 presents the aerodynamic data for the wing without nacelles configuration at 0.8 Mach number and dynamic pressures of 100, 150 and 200 psf. In this figure the lift and pitching moment curves show very little difference between the 150 and 200 psf data, but there is discernible difference in the 100 psf data. The computed lift curve slope for the 150 and 200 psf cases compare to within 1%, but the lift curve slope for the 100 psf case is 3% higher. The slope of the moment curve is 4% lower for the 100 psf case than for the

200 psf data. A similar trend is seen in the drag data with the drag steadily decreasing as dynamic pressure is increased. Again, the increment between 150 and 200 psf is noticeably smaller than the difference between 100 and 150 psf. Also note that the quadratic fit for the drag polar is much better for the 150 and 200 psf data than for the 100 psf data.

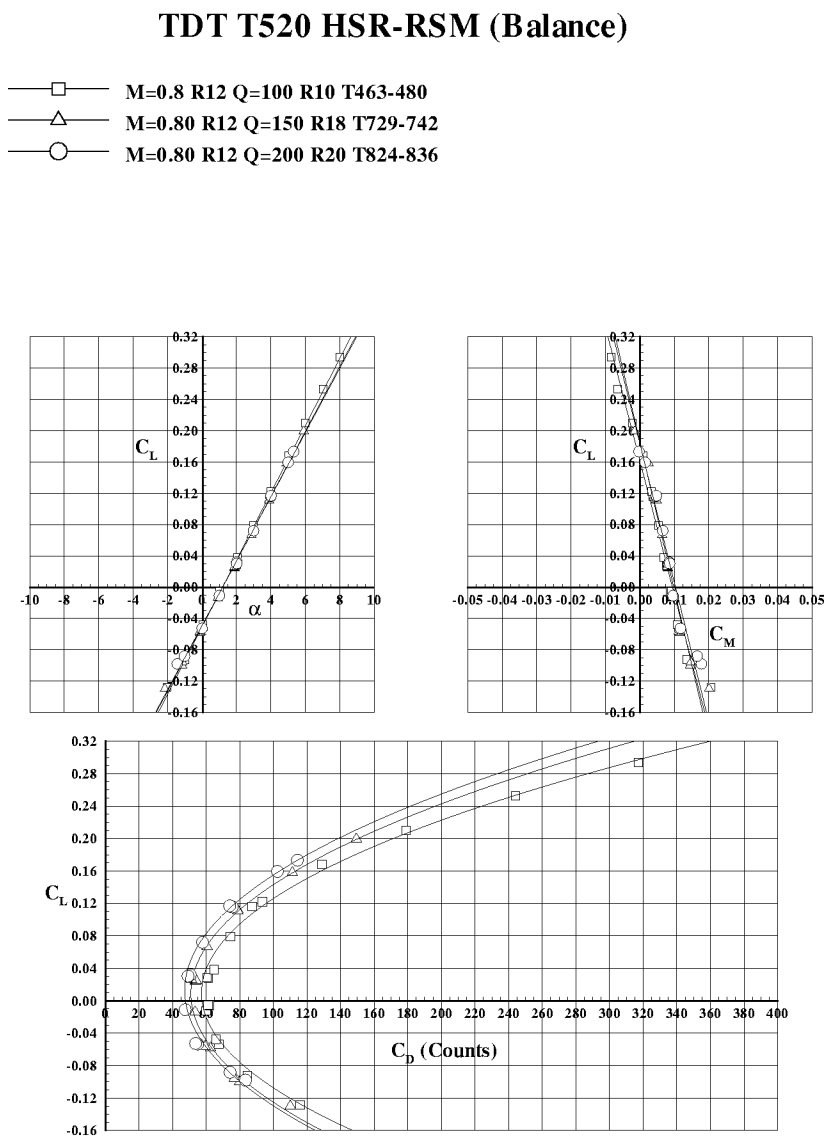

Figure 8. Aerodynamic data for various values of dynamic pressure.

The slope differences and scatter in the 100 psf data lead us to be somewhat suspicious of these data. Pure aeroelastic effects would result in a consistent change in the data as the dynamic pressure is increased. But the 150 and 200 psf data agree reasonably well, while the 100 psf is noticeably different. In addition, aeroelastic effects would not generate the scatter in the drag polar seen for the 100 psf condition. There are a number of reasons why the 100 psf data might be of lower quality than the higher dynamic pressure data. Of primary concern is the fact that the aerodynamic loads at 100 psf are two-thirds of those at 150 psf and one-half those at 200 psf. The

loads generated at 100 psf are low enough that the balance may be having problems resolving the changes from one angle-of-attack to the next. This is definitely the indication of the scatter in the drag data which is most sensitive to the resolution of the balance. The majority of data was taken at 150 psf, and from the above comparison, it appears that this value is a reasonable trade-off between data accuracy and model safety.

Loads Data as a Function of Mach Number

During TDT T520, the HSR-RSM was tested at Mach numbers ranging from 0.7 to 1.15. Figure 9 shows how the aerodynamic data vary with Mach number. The data plotted here range from Mach 0.8 to 1.15 at a dynamic pressure of 150 psf. Several well-known characteristics of aerodynamic data as a function of Mach number can be seen in these figures. Subsonically, the lift curve slope tends to increase with Mach number, eventually reaching a peak and falling back off supersonically. The slope of the moment curve decreases with Mach number illustrating the

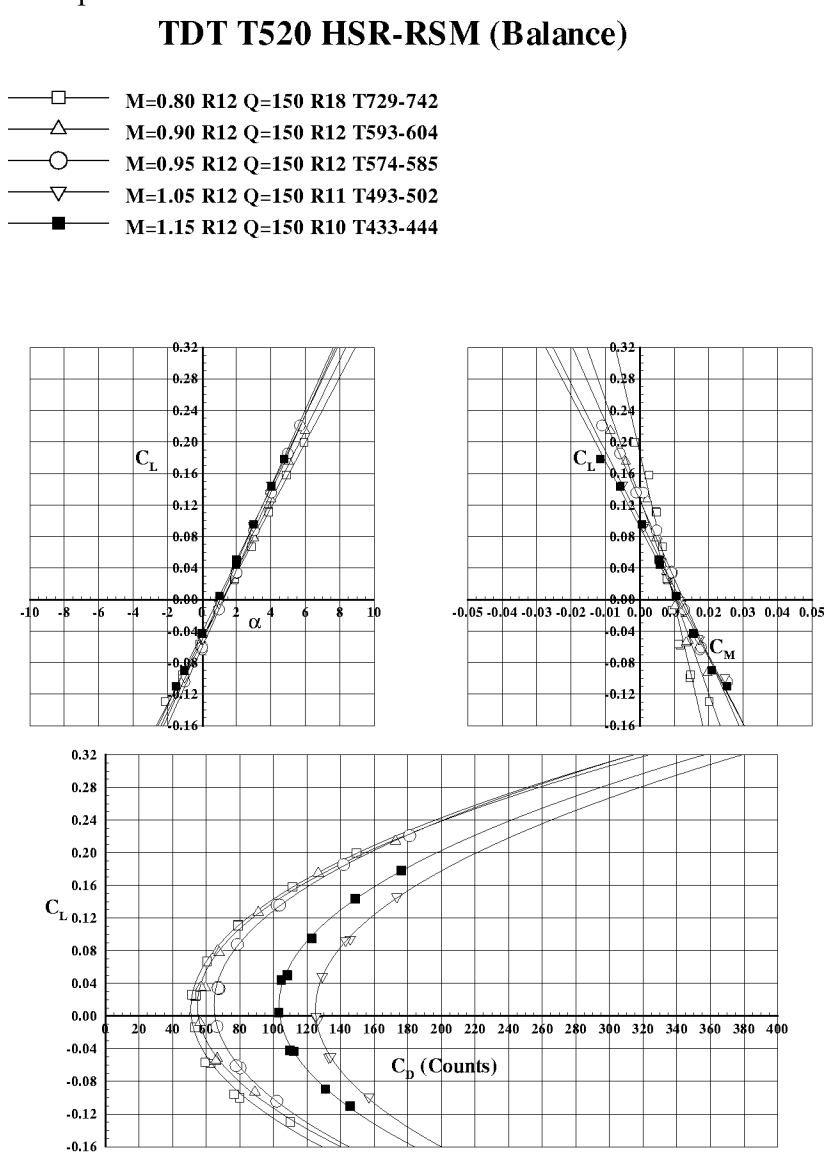

Figure 9. Aerodynamic data as a function of Mach number.

classical characteristic of an aft moving center of pressure as Mach number increases. Drag also steadily increases with Mach number, reaches a peak and falls back off supersonically. These characteristics are typical of the aerodynamic behavior of wings with increasing Mach number.

Impact of Nacelles on Wing Aerodynamics

A pair of flow-through engine nacelles representative of those included on the Reference H configuration were also tested during this wind tunnel entry. The impact of these nacelles on the aerodynamics of the vehicle at Mach 0.95 are presented in Figure 10. The addition of the nacelles shift the lift curve to the left, but it has a minimal impact on the slope of the curve. This is not surprising since the slope of the lift curve is most impacted by the wing planform. Addition of the engine nacelles effectively changes the camber distribution on the inboard portion of the wing which translates into a shift in the model lift coefficient at zero angle-of-attack. The slope of the pitching moment curve is increased with the addition of the nacelles, indicating that the nacelles

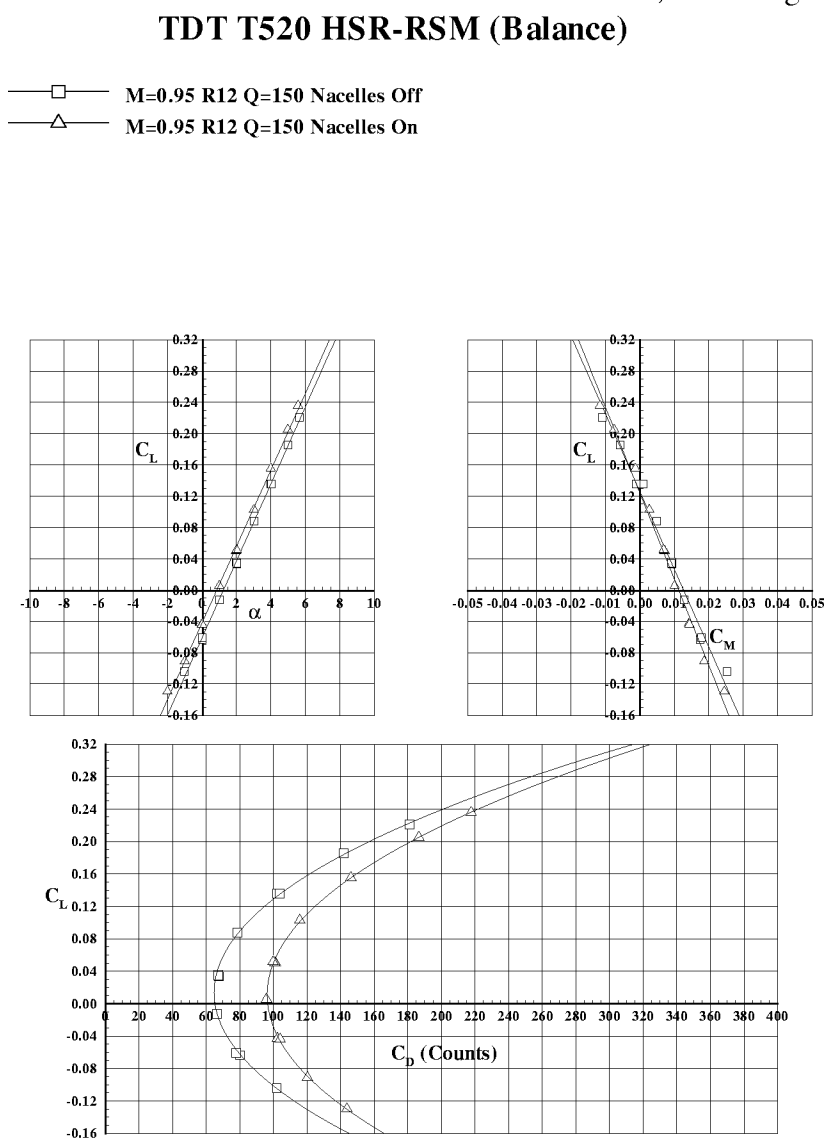

Figure 10. Comparison of clean-wing and nacelles-on data at M=0.95.

reduce the static stability of this configuration. As expected the drag increases substantially with the addition of the nacelles. Figure 11 makes a similar comparison at M=1.15. The correlation between the clean-wing and the nacelles-on data at M=1.15 are similar to the M=0.95 data in all respects.

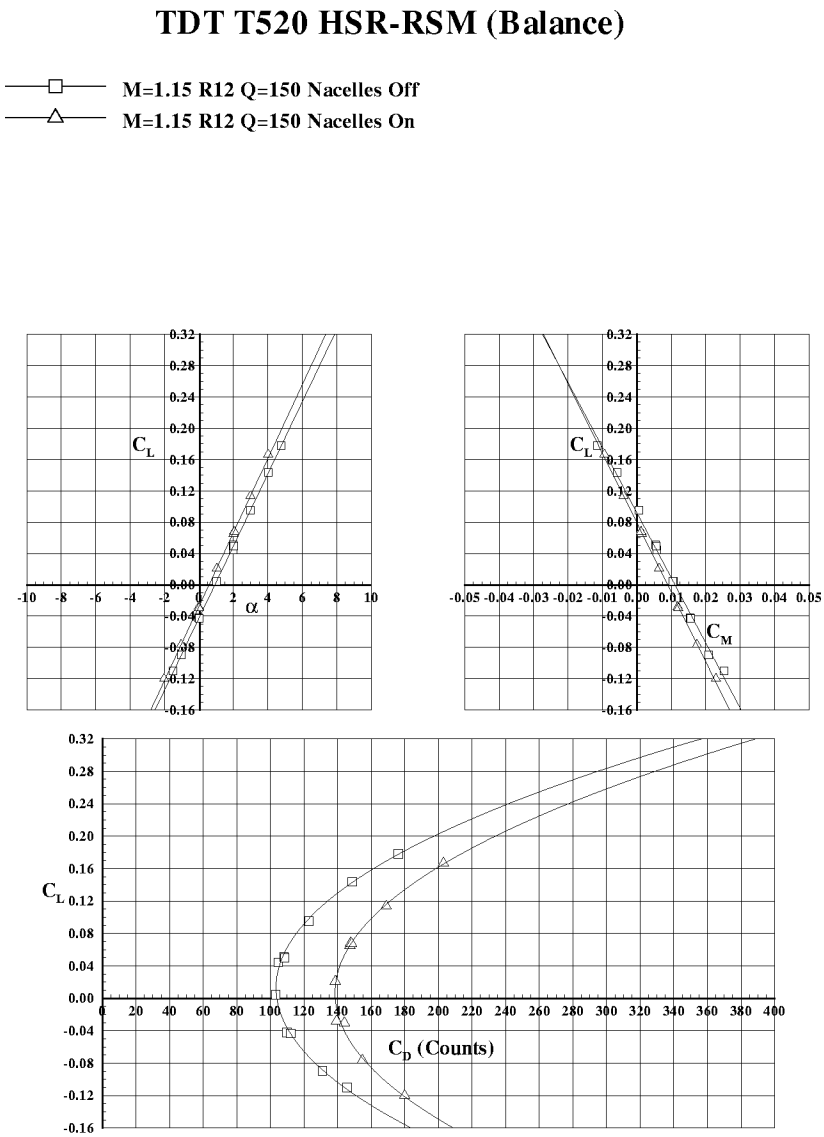

Figure 11. Comparison of clean-wing and nacelles-on data at M=1.15.

There has been considerable interest in the ability of CFD codes to be able to compute the lift and pitching moment curve slopes for this geometry as a function of Mach number. Consistently extracting this type of information from the experimental data has proven to be a task fraught with subtle problems. For instance, early wind tunnel data were fit with higher order curves, and the lift and pitching moment slopes were assumed to be the first-order coefficients in these curve fits. However, when these slopes were plotted as a function of Mach number, considerable scatter in the data was observed. Reducing the fits to linear polynomials removed a great deal of the scatter.

In addition, a great deal of data of varying quality have been taken on this configuration, and the eagerness to use these data by experimental and analytical researchers alike has resulted in a wide variation in so-called TDT experimental results for the HSR-RSM. In an effort to resolve this problem and present a set of data for use as a starting point in CFD comparisons, we have compiled what we believe to be the most consistent set of HSR-RSM TDT data for use in correlating loads computed by analytical methods. We use a linear fit of the loads data at a dynamic pressure of 150 psf. to generate plots of lift curve slope and pitching moment slope as a function of Mach number. In addition, a drag coefficient versus Mach number plot at a constant lift coefficient of 0.1 has also been developed using the drag polar fits. A plot of lift curve slope for nacelles-on and nacelles-off as a function of Mach number is presented in Figure 12. In this plot, the slopes have been fit using a cubic B-spline curve. The clean-wing lift curve slope steadily increases with Mach number up to about Mach 0.97, then it falls back off. The lift data for the nacelles-on configuration are not nearly as clean. Like the clean-wing data, we see an increase in the lift curve slope primarily in the subsonic range and a decreasing trend in the supersonic range. However, the data are somewhat scattered in the high transonic regime.

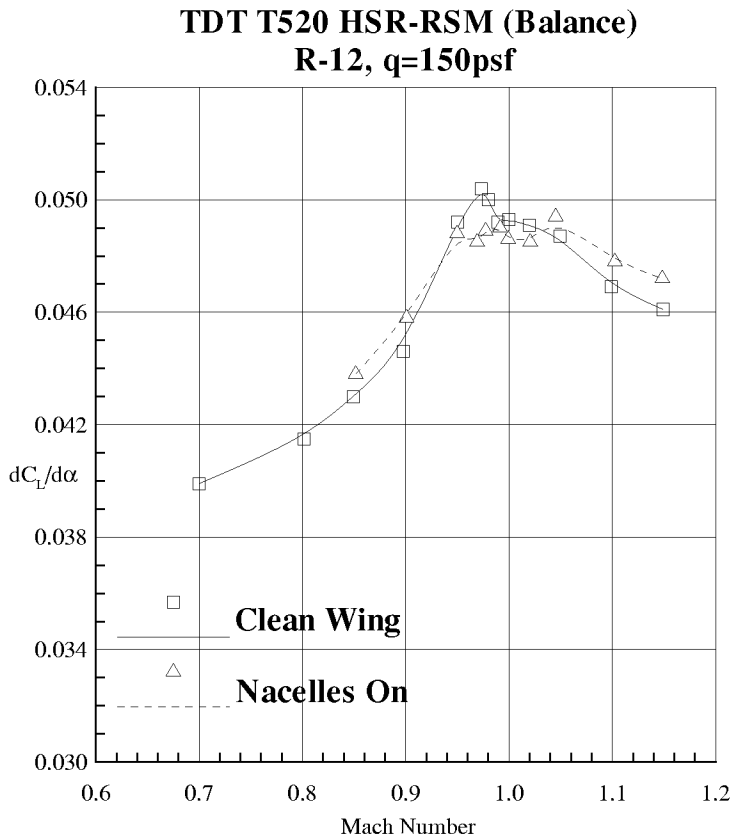

Figure 12. HSR-RSM lift curve slope as a function of Mach number.

The pitching moment curve slope as a function of Mach number is presented in Figure 13. Here the correlation between the clean-wing and nacelles-on data is somewhat better. The two curves cross at Mach 0.85, but beyond that point, they seem to maintain the same basic character. The pitching moment slope is consistently lower for the clean-wing case as was illustrated earlier. The

slope for both configurations steadily decreases as Mach number is increased, and they each have a small plateau region as they pass through the transonic range. The pitching moment slope begins to increase at M=1.15 for both configurations.

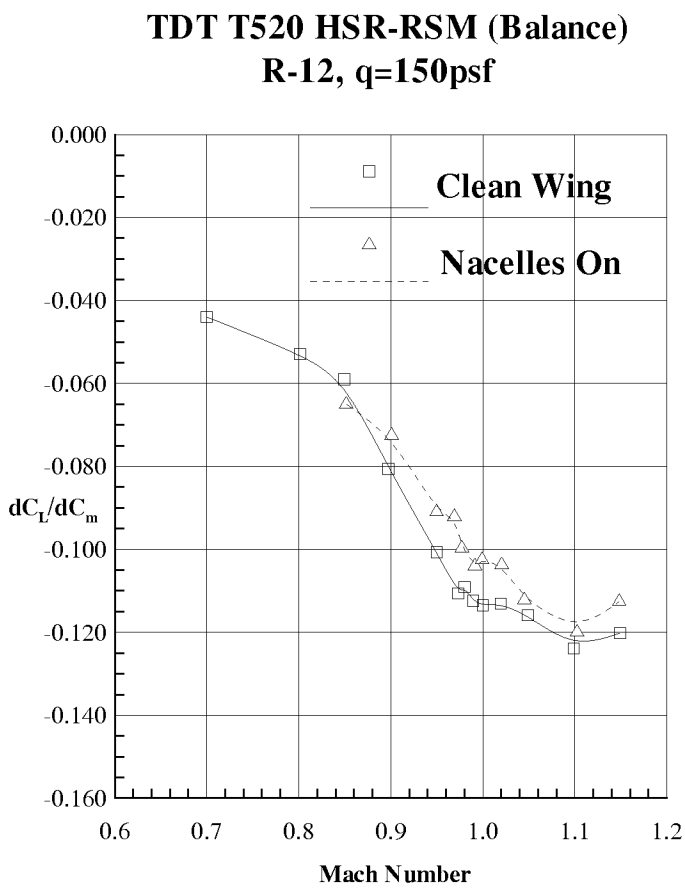

Figure 13. HSR-RSM pitching moment curve slope as a function of Mach number.

Finally, The drag coefficient at a constant lift coefficient of 0.1 is plotted against Mach number in Figure 14. Again, we see a very consistent behavior of the drag with Mach number for both the clean-wing and the wing-with-nacelles. The sharp drag rise through the transonic region is clearly displayed in this figure. The addition of the nacelles appear to have very little impact on the onset of transonic drag rise for this configuration. Both configurations appear to enter transonic drag rise at approximately 0.95 Mach number, and the drag peaks at about Mach 1.05. The addition of the nacelles increases drag by about 30 counts in the subsonic speed range and about 35 - 40 counts at supersonic speeds.

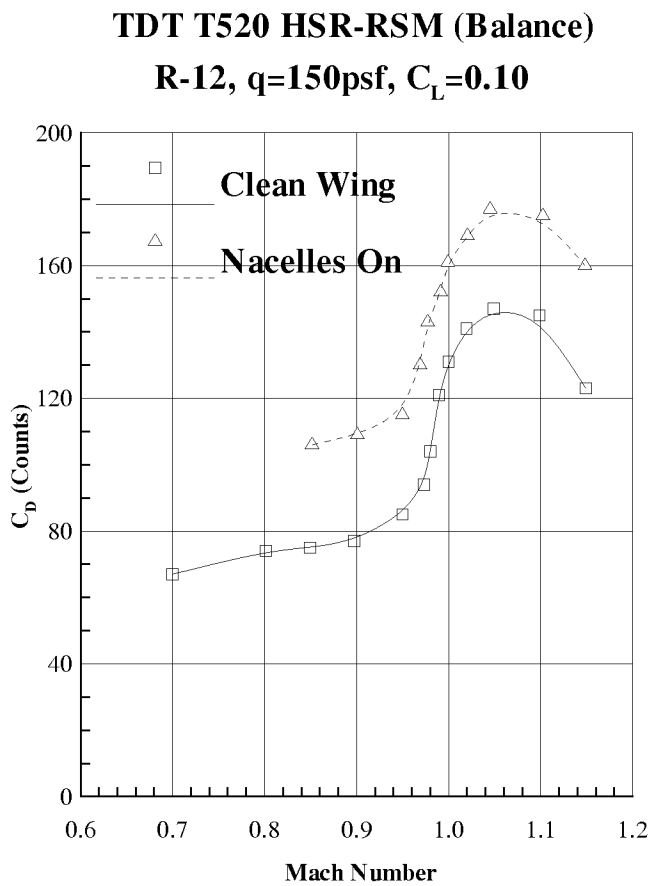

Figure 14. HSR-RSM drag coefficient at C_L = 0.1 as a function of Mach number.

Aerodynamic Response to Control Surface Deflection

Aerodynamic data were acquired as a function of flap deflection at constant angle-of-attack for both the clean-wing and wing-with-nacelles configurations. Steady deflected flap and oscillating flap data were taken at Mach numbers ranging from 0.8 to 1.10. The majority of data were acquired at a dynamic pressure of 150 psf, but selected data were also taken at 100 and 200 psf. Time history records for the oscillating flap cases are available in digital form, but only the steady deflected flap data are discussed in this report.

Figure 15 shows the response of the HSR-RSM lift, pitching moment, and drag due to flap deflection for a Mach number range of 0.85 to 1.10. This plot is very enlightening since it presents an extremely wide variation in control surface effectiveness with Mach number. The lift curve slope at Mach 1.10 is less than half that at Mach 0.95. This variation is very likely due to shock interaction with the control surface in the transonic range. Examining the lift coefficient versus angle-of-attack plot, an increase in the lift curve slope is observed between Mach 0.85 and 0.95, but beyond Mach 0.95, the lift curve slope decreases dramatically. Looking back at Figure 14, we see that transonic drag rise for this configuration occurs between Mach 0.95 and 1.05. It is in this range that shocks form on the surface of the wing and steadily move aft with increasing Mach number, eventually reaching the wing trailing edge at supersonic speeds. This supports the

assumption that the loss in control effectiveness is due to shock interaction with the control surface. The pitching moment data show similar trends with the slope steadily decreasing with increasing Mach number.

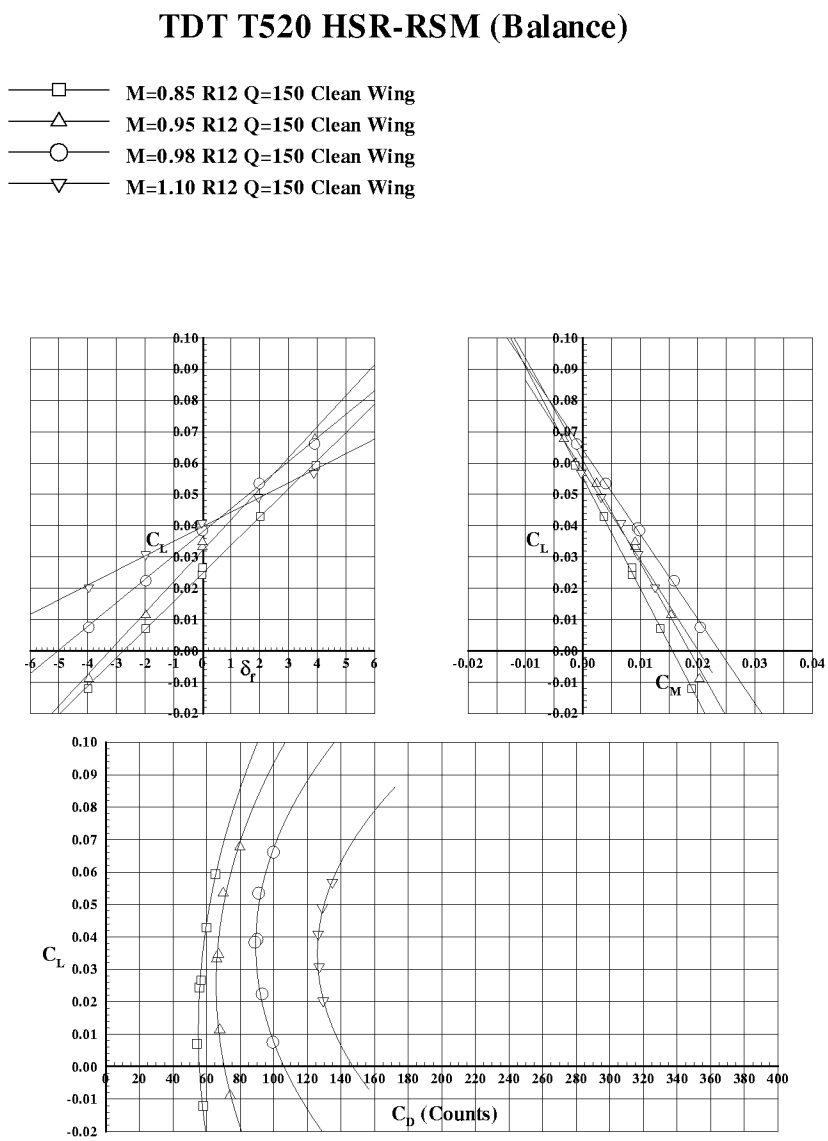

Figure 15. HSR-RSM clean-wing steady flap deflection data.

Finally, Figure 16 shows the steady flap deflection loads for the wing with the nacelles. The trends observed in this plot are similar to those for the clean-wing data except for the drag polar. The wing-with-nacelles data show a noticeable increase in the lift coefficient for minimum drag as Mach number increases. However, one should probably use caution when interpreting these data due to the limitation on flap deflections which could be performed with the nacelles on the wing. Interference between the inboard nacelle and the flap precluded testing with positive flap deflection angles. Therefore, these data, especially the drag, may be unduly biased by the fact that only data due to negative flap deflection angles could be obtained.

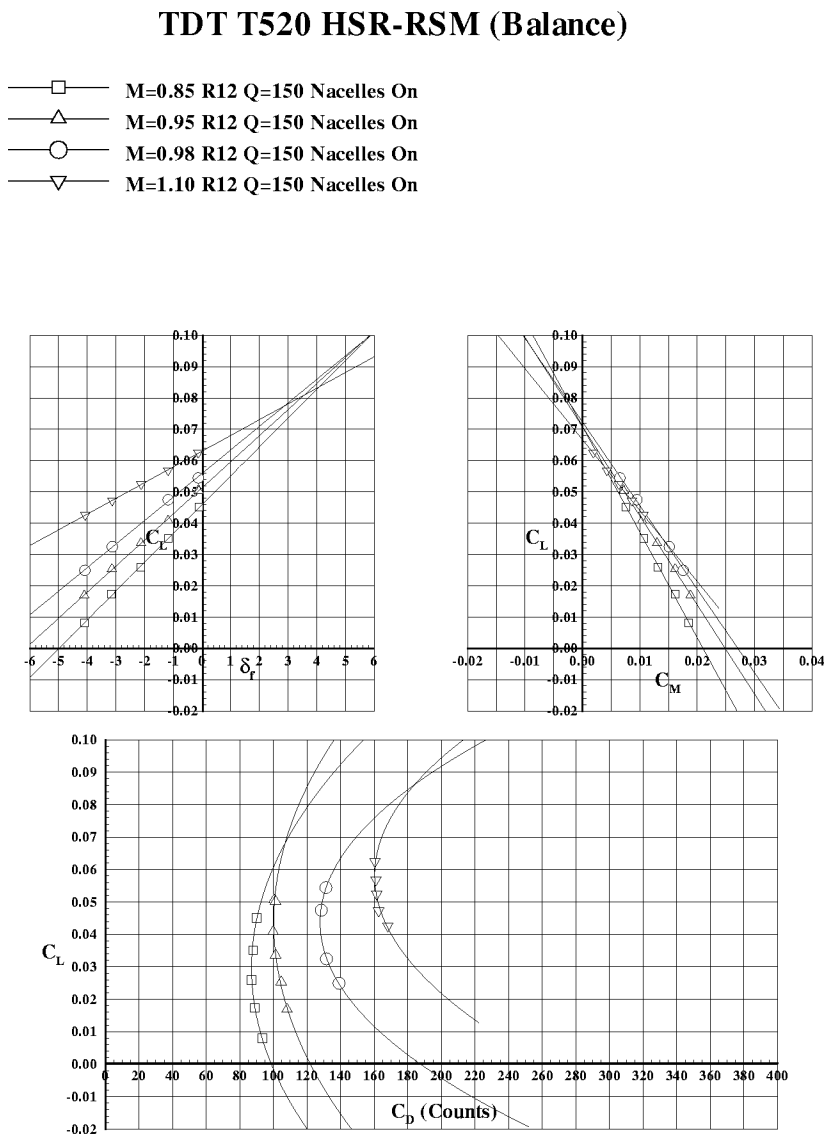

Figure 16. HSR-RSM wing-with-nacelles steady flap deflection data.

Pressure Data Acqisition and Reduction

Wing and fuselage pressure data were acquired for each polar presented in Table 3. For each tab point unsteady pressure data were acquired and time averaged to obtain a mean pressure and maximum and minimum pressure fluctuation for each point on the surface of the wing. Simultaneously, steady fuselage pressures were obtained using a separate data system. Both the wing and fuselage data were then processed into ASCII channel statistics files and stored for future post processing. The wing pressure transducer calibrations were checked before each run by applying a known constant pressure to the reference side of each transducer and recording the pressure reading. Transducers were calibrated if the error between the actual and measured pressure was greater than 3%. The fuselage pressure calibrations were found to be very stable.

These transducers were simply calibrated on a periodic basis, typically immediately after the initial warm-up run at the beginning of a day of testing. Prior to and following each run, a wind off zero was taken and the pressure reading of each transducer was recorded. This allowed us to monitor the health of each transducer over the period of the run and also provided guidance for determining when the transducers might require calibration. The wind off zero before each run is also used as a basis for reducing the raw pressure data that is included in the channel statistics file.

The channel statistics files for each tab point are tabulated and processed using a Microsoft Excel™ macro. The wing pressure output from this macro for a single tab point is shown in Figure 17. For each tab point, tunnel conditions are summarized, pressure data organized along wing chords are tabulated, and the wing pressure coefficient as a function of percentage of local wing chord is plotted. In addition, the wing pressure coefficient at 20% wing chord is plotted as a function of wing semispan. The pressure differential between the upper and lower surface of the wing is calculated for each chord and is also tabulated and plotted in this figure. Note that the aerodynamic loads tabulated in these charts were normalized by different areas and reference lengths than those reported elsewhere in this document. The aerodynamic loads printed by the pressure-data macros should only be used for comparison with like-macro output.

Figure 18 is a similar output for the fuselage pressure data. Since the fuselage pressure instrumentation measures steady pressure, only the mean pressure coefficient at each fuselage station is tabulated. The fuselage pressure data are organized along constant fuselage cuts and are tabulated and plotted as a function of the azimuthal angle measured from the TDT wall on the upper surface of the fuselage to the TDT wall on the lower surface of the fuselage.

The output from both the wing and fuselage macros, as well as all of the channel statistics files for each run and tab point taken during this test have been compiled into a CD-ROM volume. Copies of this volume have been previously distributed to the HSR industry partners. As with the force data, we will summarize important aspects of the pressure data, especially in light of some of the findings from the force data, rather than provide an exhaustive listing of all of the wing and fuselage pressure data.

Run	10	TDT Test # 520 HSR RSM-Bal
Tab	408	Pressure Distribution Statistics

Mach	q (psf)	Re (10**6/ft)	γ	α (deg)
0.951	102.9	1.66	1.138	-2.00

Aileron Position (deg.)

	Cmd.	Pos.
Mean	0.00	-0.02
Amplitude (1/2 P-P)	0.01	0.01

Tunnel Conditions

H (psf)	P (psf)	T (deg F)	R-12 Purity
329.3	199.8	82.9	0.95

Aileron Hinge Moment (in-lbs.)

Max.	Min.	Mean
36.20	-17.25	8.42

Lift Force Coeff.	Pitching Moment Coeff.	Drag Force Coeff.	Rolling Moment Coeff.	Yawing Moment Coeff.
-0.0798	0.0899	0.0080	-0.0233	0.0006

Acquired 28 MAR 96 at 10:14:06
Adjusted using wind-off zero Tab # 403
500 samples/second for 5 seconds
Samples 1 through 2500; 100.00% of 2500 samples

Upper surface 0.10 semispan

x/c	Cp Mean	Cp Min	Cp Max	Std Dev	Chan
0.000	-0.02	-0.05	0.01	0.01	151
0.025	0.03	0.01	0.05	0.01	186
0.050	0.05	0.03	0.07	0.01	152
0.100	0.07	0.04	0.09	0.01	153
0.150	0.06	0.04	0.07	0.01	154
0.200	0.01	0.00	0.03	0.01	155
0.250	0.00	-0.02	0.02	0.01	156
0.300	-0.01	-0.03	0.01	0.01	157
0.350	0.01	-0.01	0.02	0.01	158
0.400	0.01	-0.01	0.03	0.01	159
0.450	0.02	0.00	0.04	0.01	160
0.500	0.00	-0.02	0.02	0.01	161
0.550	0.00	-0.02	0.02	0.01	162
0.600	0.01	0.00	0.03	0.01	163
0.650	-0.02	-0.04	0.00	0.01	164
0.700	-0.02	-0.04	0.00	0.01	165
0.750	-0.02	-0.04	0.01	0.01	166
0.800	0.00	-0.02	0.03	0.01	167
0.850	0.01	-0.02	0.03	0.01	168

Lower surface 0.10 semispan

x/c	Cp Mean	Cp Min	Cp Max	Std Dev	Chan	Delta-Cp
0.025	-0.09	-0.11	-0.06	0.01	187	- 0.113
0.050	-0.04	-0.08	-0.02	0.01	169	- 0.094
0.100	-0.03	-0.05	-0.01	0.01	170	- 0.094
0.150	0.00	-0.02	0.02	0.01	171	- 0.057
0.200	-0.02	-0.04	0.00	0.01	172	- 0.033
0.250	-0.03	-0.05	-0.01	0.01	173	- 0.028
0.300	0.73	0.71	0.75	0.01	174	0.738
0.350	-0.04	-0.06	-0.02	0.01	175	- 0.042
0.400	-0.05	-0.07	-0.03	0.01	176	- 0.065
0.450	-0.08	-0.10	-0.05	0.01	177	- 0.099
0.500	-0.09	-0.11	-0.06	0.01	178	- 0.085
0.550	0.01	0.01	0.01	0.01	179	0.011
0.600	-0.14	-0.16	-0.12	0.01	180	- 0.152
0.650	-0.21	-0.24	-0.18	0.01	181	- 0.190
0.700	-0.18	-0.21	-0.15	0.01	182	- 0.157
0.750	-0.21	-0.24	-0.18	0.01	183	- 0.192
0.800	-0.28	-0.31	-0.26	0.01	184	- 0.283
0.850	-0.34	-0.37	-0.30	0.01	185	- 0.348

Upper surface 0.30 semispan

x/c	Cp Mean	Cp Min	Cp Max	Std Dev	Chan
0.000	0.00	-0.04	0.02	0.01	111
0.025	0.08	0.06	0.10	0.01	145
0.050	0.06	0.05	0.08	0.01	112
0.100	0.28	0.17	0.37	0.04	113
0.150	0.05	0.03	0.07	0.01	114
0.200	0.03	0.02	0.05	0.01	115
0.250	0.01	-0.01	0.04	0.01	116
0.300	0.01	-0.01	0.04	0.01	117
0.350	0.06	0.04	0.08	0.01	118
0.400	0.04	0.02	0.07	0.01	119
0.450	0.04	0.02	0.06	0.01	120
0.500	-0.02	-0.04	0.00	0.01	121
0.550	0.00	-0.02	0.03	0.01	122
0.600	-0.02	-0.05	0.01	0.01	123
0.650	-0.01	-0.04	0.02	0.01	124
0.700	0.01	-0.01	0.05	0.01	125
0.750	0.01	-0.01	0.05	0.01	126
0.800	0.00	-0.02	0.03	0.01	127

Lower surface 0.30 semispan

x/c	Cp Mean	Cp Min	Cp Max	Std Dev	Chan	Delta-Cp
0.025	-0.34	-0.40	-0.30	0.02	146	- 0.424
0.050	-0.23	-0.30	-0.16	0.02	129	- 0.294
0.100	-0.11	-0.12	-0.11	0.00	130	- 0.397
0.150	-0.06	-0.09	-0.04	0.01	131	- 0.111
0.200	-0.08	-0.11	-0.06	0.01	132	- 0.118
0.250	-0.08	-0.11	-0.06	0.01	133	- 0.095
0.300	-0.10	-0.12	-0.07	0.01	134	- 0.110
0.350	-0.10	-0.12	-0.08	0.01	135	- 0.160
0.400	-0.14	-0.15	-0.12	0.01	136	- 0.178
0.450	-0.19	-0.21	-0.17	0.01	137	- 0.230
0.500	-0.19	-0.22	-0.16	0.01	138	- 0.163
0.550	-0.16	-0.19	-0.14	0.01	139	- 0.163
0.600	-0.19	-0.22	-0.17	0.01	140	- 0.168
0.650	-0.24	-0.27	-0.21	0.01	141	- 0.223
0.700	-0.32	-0.35	-0.30	0.01	142	- 0.336
0.750	-0.45	-0.47	-0.44	0.01	143	- 0.465
0.800	-0.48	-0.51	-0.45	0.01	144	- 0.477

Figure 17. Output from the wing pressure package macro.

Run	10	TDT Test # 520 HSR RSM-Bal
Tab	408	Pressure Distribution Statistics

Mach	q (psf)	Re (10**6/ft)	γ	α (deg)
0.951	102.9	1.66	1.138	-2.00

Aileron Position (deg.)

	Cmd.	Pos.
Mean	0.00	-0.02
Amplitude (1/2 P-P)	0.01	0.01

Tunnel Conditions

H (psf)	P (psf)	T (deg F)	R-12 Purity
329.3	199.8	82.9	0.95

Aileron Hinge Moment (in-lbs.)

Max.	Min.	Mean
36.20	-17.25	8.42

Lift Force Coeff.	Pitching Moment Coeff.	Drag Force Coeff.	Rolling Moment Coeff.	Yawing Moment Coeff.
-0.0798	0.0899	0.0080	-0.0233	0.0006

Acquired 28 MAR 96 at 10:14:06
Adjusted using wind-off zero Tab # 403
500 samples/second for 5 seconds
Samples 1 through 2500; 100.00% of 2500 samples

Upper surface 0.60 semispan

x/c	Cp Mean	Cp Min	Cp Max	Std Dev	Chan
0.000	-0.54	-0.63	-0.43	0.03	65
0.050	0.28	0.26	0.30	0.01	66
0.100	0.15	0.13	0.17	0.01	67
0.150	0.11	0.09	0.14	0.01	68
0.200	0.08	0.06	0.11	0.01	69
0.250	0.07	0.05	0.10	0.01	70
0.300	0.04	0.02	0.08	0.01	71
0.350	0.01	-0.01	0.06	0.01	72
0.400	0.00	-0.02	0.05	0.01	73
0.450	-0.02	-0.05	0.04	0.01	74
0.500	-0.05	-0.07	0.02	0.01	75
0.550	-0.06	-0.09	0.01	0.01	76
0.600	-0.08	-0.11	-0.01	0.01	77
0.650	-0.10	-0.14	-0.02	0.02	78
0.700	-0.11	-0.16	-0.03	0.02	79
0.750	-0.08	-0.13	-0.01	0.02	80
0.800	-0.10	-0.17	-0.02	0.03	81
0.850	-0.08	-0.17	-0.02	0.02	82
0.900	-0.04	-0.09	0.01	0.02	83
0.950	0.05	0.01	0.09	0.01	84
1.000	0.17	0.14	0.21	0.01	85

Lower surface 0.60 semispan

x/c	Cp Mean	Cp Min	Cp Max	Std Dev	Chan	Delta-Cp
0.050	-0.74	-0.86	-0.62	0.04	86	- 1.013
0.100	-0.57	-0.66	-0.47	0.03	87	- 0.713
0.150	-0.30	-0.36	-0.21	0.02	88	- 0.417
0.200	-0.22	-0.27	-0.17	0.02	89	- 0.301
0.250	-0.23	-0.27	-0.18	0.01	90	- 0.297
0.300	-0.22	-0.25	-0.19	0.01	91	- 0.258
0.350	-0.26	-0.29	-0.23	0.01	92	- 0.267
0.400	-0.28	-0.30	-0.25	0.01	93	- 0.276
0.450	-0.30	-0.33	-0.28	0.01	94	- 0.280
0.500	-0.34	-0.37	-0.32	0.01	95	- 0.294
0.550	-0.37	-0.39	-0.34	0.01	96	- 0.306
0.600	-0.41	-0.43	-0.39	0.01	97	- 0.331
0.650	-0.45	-0.47	-0.43	0.01	98	- 0.346
0.700	-0.49	-0.51	-0.47	0.01	99	- 0.377
0.750	-0.49	-0.51	-0.47	0.01	100	- 0.406
0.800	-0.53	-0.55	-0.50	0.01	101	- 0.427
0.850	-0.33	-0.54	-0.10	0.09	102	- 0.248
0.900	0.01	-0.10	0.07	0.02	103	0.043
0.950	0.10	0.05	0.14	0.01	104	0.053

Upper Surface 0.95 Semispan

x/c	Cp Mean	Cp Min	Cp Max	Std Dev	Chan
0.000	-1.33	-1.38	-1.27	0.03	31
0.100	0.13	0.10	0.17	0.01	32
0.200	-0.02	-0.06	0.03	0.02	33
0.300	-0.09	-0.12	-0.04	0.02	34
0.400	-0.12	-0.17	-0.06	0.02	35
0.500	-0.14	-0.20	-0.06	0.03	36
0.600	-0.19	-0.26	-0.08	0.03	37
0.700	-0.23	-0.34	-0.08	0.07	38
0.800	-0.09	-0.23	-0.02	0.03	39
0.900	0.02	-0.04	0.07	0.02	40

Lower Surface 0.95 Semispan

x/c	Cp Mean	Cp Min	Cp Max	Std Dev	Chan	Delta-Cp
0.100	-0.77	-0.84	-0.73	0.02	42	- 0.902
0.200	-0.69	-0.71	-0.66	0.02	43	- 0.666
0.300	-0.58	-0.61	-0.54	0.01	44	- 0.490
0.400	-0.52	-0.56	-0.48	0.02	45	- 0.400
0.500	-0.47	-0.53	-0.36	0.03	46	- 0.329
0.600	-0.36	-0.48	-0.26	0.05	47	- 0.168
0.700	-0.22	-0.49	-0.11	0.06	48	0.015
0.800	-0.07	-0.19	-0.01	0.03	49	0.017
0.900	0.02	-0.04	0.06	0.02	50	- 0.007

Upper Surface 0.20 Chord

2y/b	Cp Mean	Cp Min	Cp Max	Std Dev	Chan
0.100	0.01	0.00	0.03	0.01	155
0.200	0.02	0.00	0.04	0.01	147
0.300	0.03	0.02	0.05	0.01	115
0.450	0.06	0.05	0.08	0.01	105
0.600	0.08	0.06	0.11	0.01	69
0.750	0.02	0.00	0.06	0.01	62
0.950	-0.02	-0.06	0.03	0.02	33

Lower Surface 0.20 Chord

2y/b	Cp Mean	Cp Min	Cp Max	Std Dev	Chan	Delta-Cp
0.100	-0.02	-0.04	0.00	0.01	172	- 0.033
0.200	0.00	0.00	0.00	0.00	148	- 0.015
0.300	-0.08	-0.11	-0.06	0.01	132	- 0.118
0.450	-0.34	-0.38	-0.30	0.01	106	- 0.402
0.600	-0.22	-0.27	-0.17	0.02	89	- 0.301
0.750	-0.48	-0.55	-0.42	0.02	63	- 0.508
0.950	-0.69	-0.71	-0.66	0.02	43	- 0.666

Figure 17(Continued). Output from the wing pressure package macro.

Run	10	TDT Test # 520 HSR RSM-Bal
Tab	408	Pressure Distribution Statistics

Mach	q (psf)	Re (10**6/ft)	γ	α (deg)
0.951	102.9	1.66	1.138	-2.00

Aileron Position (deg.)	Cmd.	Pos.
Mean	0.00	-0.02
Amplitude (1/2 P-P)	0.01	0.01

Lift Force Coeff.	Pitching Moment Coeff.	Drag Force Coeff.	Rolling Moment Coeff.	Yawing Moment Coeff.
-0.0798	0.0899	0.0080	-0.0233	0.0006

Acquired 28 MAR 96 at 10:14:06
Adjusted using wind-off zero Tab # 403
500 samples/second for 5 seconds
Samples 1 through 2500; 100.00% of 2500 samples

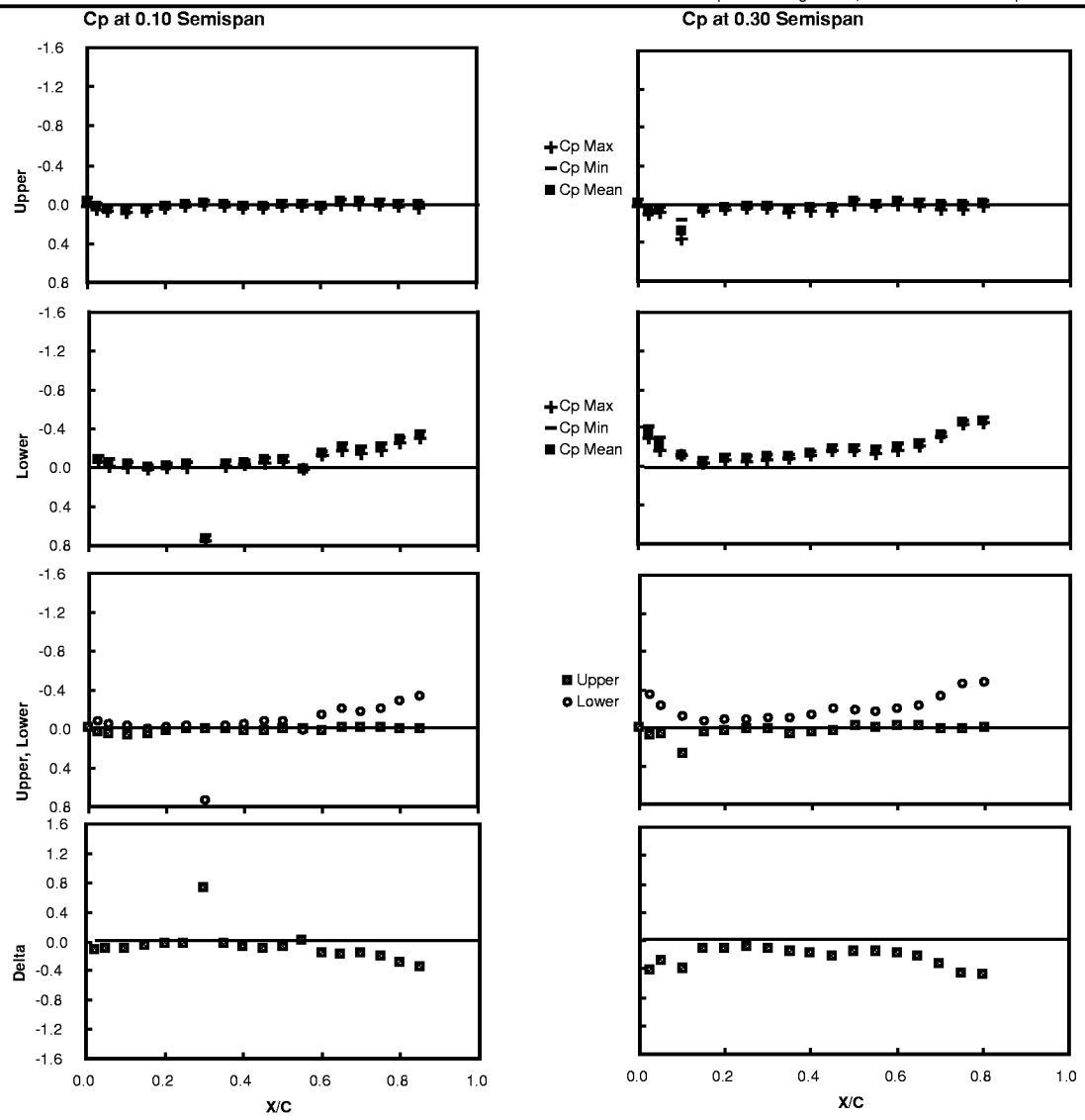

Figure 17(Continued). Output from the wing pressure package macro.

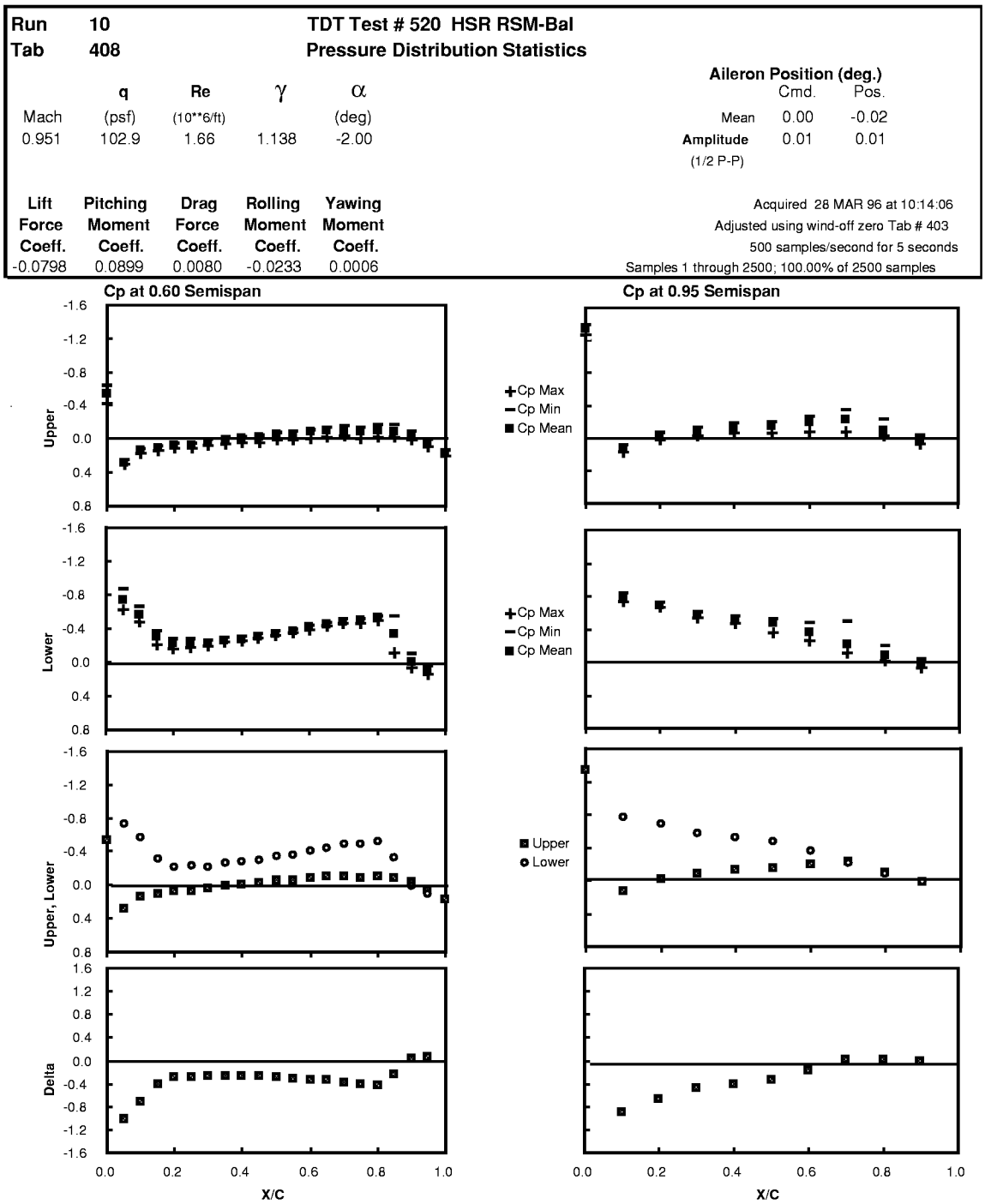

Figure 17(Continued). Output from the wing pressure package macro.

Run	10	TDT Test # 520 HSR RSM-Bal			
Tab	408	Pressure Distribution Statistics			

	q	Re	γ	α
Mach	psi	(10**6/ft)		(deg)
0.951	102.9	1.66	1.138	-2.00

Lift Force Coeff.	Pitching Moment Coeff.	Drag Force Coeff.	Rolling Moment Coeff.	Yawing Moment Coeff.
-0.0798	0.0899	0.0080	-0.0233	0.0006

Aileron Position (deg.)

	Cmd.	Pos.
Mean	0.00	-0.02
Amplitude (1/2 P-P)	0.01	0.01

Acquired 28 MAR 96 at 10:14:06
Adjusted using wind-off zero Tab # 403
500 samples/second for 5 seconds
Samples 1 through 2500; 100.00% of 2500 samples

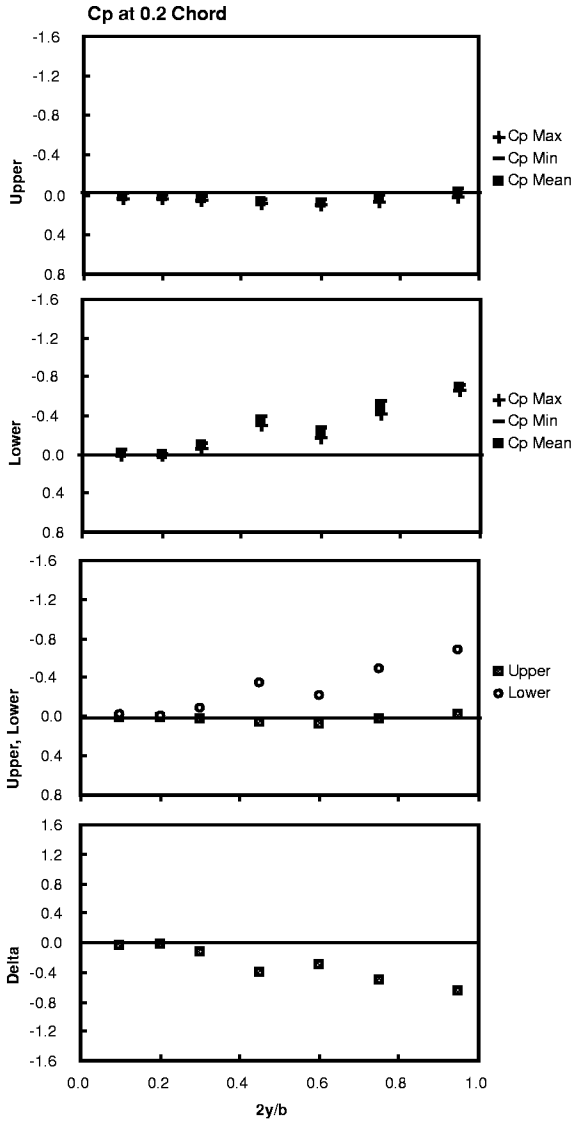

Figure 17(Continued). Output from the wing pressure package macro.

Run **10** **TDT Test #520 HSR RSM-Bal**

Tab **408** **Fuselage Pressures**

Mach	q (psf)	α (deg)
0.952	102.90	−2.00

Acquired on Mar 28, 1996 at 10:14 AM

100 Sample Sets Acquired at a Sample Rate of 20 Khz

Fuselage Stations

Theta Measured from Upper Fuselage Symmetry Plane

X = 16"			X = 36"			X = 60"			X = 102"		
Theta	Cp Mean	Chan	Theta	Cp Mean	Chan	Theta	Cp Mean	Chan	Theta	Cp Mean	Chan
9.23	−0.20	1	7.97	0.01	17	7.97	0.01	33	54.00	−0.02	49
13.78	−0.22	2	15.64	0.01	18	15.64	0.01	34	57.13	−0.02	50
18.22	−0.21	3	22.78	0.01	19	22.78	0.01	35	60.23	−0.02	51
26.56	−0.24	4	35.26	0.01	20	35.26	0.01	36	63.30	−0.02	52
40.71	−0.23	5	54.00	0.01	21	54.00	0.02	37	66.36	−0.01	53
47.33	−0.33	6	66.36	0.01	22	66.36	0.05	38	67.93	−0.01	54
80.99	−0.25	7	79.81	0.01	23	79.81	0.14	39	69.53	−0.01	55
90.00	−0.25	8	90.00	0.01	24	90.00	0.34	40	71.17	−0.02	56
99.01	−0.25	9	100.19	0.01	25	100.19	0.09	41	108.83	−0.03	57
132.67	−0.32	10	113.64	0.01	26	113.64	0.03	42	110.47	−0.04	58
139.29	−0.30	11	126.00	0.01	27	126.00	0.01	43	112.07	−0.04	59
153.44	−0.29	12	144.74	0.01	28	144.74	0.00	44	113.64	−0.04	60
161.78	−0.30	13	157.22	0.01	29	157.22	0.00	45	119.77	−0.04	61
166.22	−0.30	14	164.36	0.01	30	164.36	0.00	46	122.87	−0.04	62
170.77	−0.29	15	172.03	0.01	31	172.03	0.01	47	126.00	−0.04	63

X = 132" (Upper)			X =132" (Lower)			X = 182"			X = 204"		
Theta	Cp Mean	Chan	Theta	Cp Mean	Chan	Theta	Cp Mean	Chan	Τηετα	Cp Mean	Chan
7.97	0.02	65	107.16	−0.16	81	7.97	0.01	97	7.97	−0.08	113
15.64	0.02	66	108.83	−0.17	82	15.64	0.01	98	15.64	−0.08	114
22.78	0.02	67	110.47	−0.18	83	22.78	0.01	99	22.78	−0.08	115
29.24	0.02	68	112.07	−0.16	84	35.26	0.02	100	35.26	−0.09	116
35.26	0.02	69	113.64	−0.16	85	54.00	0.03	101	54.00	−0.08	117
41.43	0.02	70	116.70	−0.17	86	66.36	0.05	102	66.36	−0.08	118
54.00	−0.01	71	119.77	−0.18	87	79.81	0.05	103	79.81	−0.08	119
57.13	−0.01	72	122.87	−0.17	88	90.00	0.06	104	90.00	−0.09	120
60.23	−0.01	73	126.00	−0.15	89	100.19	0.01	105	100.19	−0.09	121
63.30	−0.02	74	138.57	−0.16	90	113.64	0.00	106	113.64	−0.09	122
66.36	−0.02	75	144.74	−0.17	91	126.00	0.00	107	126.00	−0.10	123
67.93	−0.02	76	150.76	−0.25	92	144.74	−0.03	108	144.74	−0.09	124
69.53	−0.03	77	157.22	−0.15	93	157.22	−0.05	109	157.22	−0.09	125
71.17	−0.04	78	164.36	−0.14	94	164.36	−0.05	110	164.36	−0.11	126
			172.03	−0.15	95	172.03	−0.06	111	172.03	−0.10	127

Figure 18. Output from the fuselage pressure package macro.

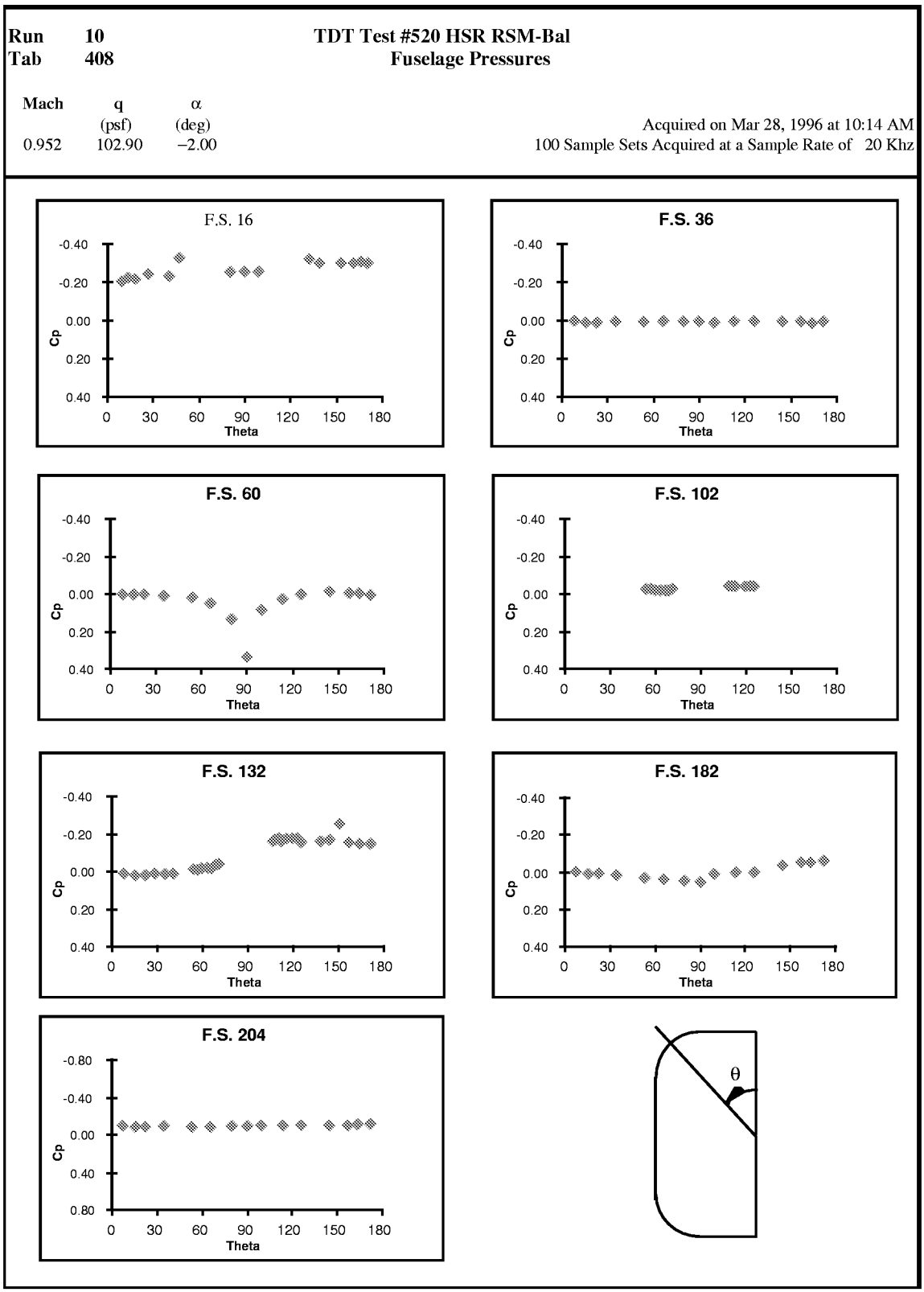

Figure 18(Continued). Output from the fuselage pressure package macro.

Effect of Wall Slots on Pressure Data

Returning to Figure 6 which compared loads data at Mach 0.8 with the TDT east wall slots open and closed, we observed that the lift-curve slope is higher for the slots closed data than for the data with the slots open. This result is further amplified by examining the pressure data presented in Figure 19. Here the wing surface pressure data are plotted at the four constant span stations as a function of the local chordwise location on the wing surface. These data represent the six degree angle-of-attack load condition presented in Figure 6. Examination of the pressure data verifies that the slots-closed configuration generates more lift at these conditions. The figure also shows that the slots have the largest impact on the upper surface pressures. Somewhat counter-intuitively, the effect of the slots is not localized to the inboard sections of the wing. Significant differences in the pressures are observed as far spanwise as 60% semispan. At 95% span, the slots seem to have minimal impact on the pressure distribution. It is interesting to note that previous flow visualization using tufts indicate that a leading edge vortex is present on the outer wing panel, and this vortex can be identified as the large suction region on the forward part of the airfoil at the 60% span station. This portion of the flowfield appears to be especially affected by whether the wind tunnel wall slots are open or closed. Based purely on these pressure-distribution data, running with the slots open seems to significantly reduce the strength of the leading edge vortex.

Pressure Data as a Function of Dynamic Pressure

Figure 8 showed that the loads data at Mach 0.8 and a dynamic pressure of 100 psf are in disagreement with the data at 150 and 200 psf. Examination of the pressure data at Mach 0.8, 5 degrees angle-of-attack and dynamic pressures of 100, 150 and 200 psf, shown in Figure 20, provides valuable insight into what is happening at these conditions. Except for a few isolated points on the inboard section, the pressure distributions at the three dynamic pressures compare very favorably at 10, 30 and 60% span. However, at 95% span the pressure distribution at 100 psf is drastically different from those at 150 and 200 psf. A number of issues pertaining to static aeroelastic concerns can be quickly addressed using these data. First the overall consistency of the data on the inboard sections of the wing leads one to conclude that the mounting system for the wing is not deflecting significantly under aerodynamic load. Likewise, we can conclude that the wing itself is not significantly deflecting under aerodynamic load since even the lower surface pressures at 95% span are very consistent from one dynamic pressure to the next. If the difference in the upper surface pressures were due to static aeroelastic effects, similar trends would also be seen in the lower surface pressures. Absence of these differences indicate that static aeroelasticity is likely not a concern with this model.

Given the above conclusions, the difference in the upper surface pressure at 95% span appears to be a local anomaly in the flowfield. It is speculated that this difference may be a function of transition, or possibly flow separation in the vicinity of the wing tip. Cross correlation with data at other Mach numbers, and possibly flow-visualization data, might provide further insight into this feature. Unfortunately, these studies are well beyond the scope of the present report.

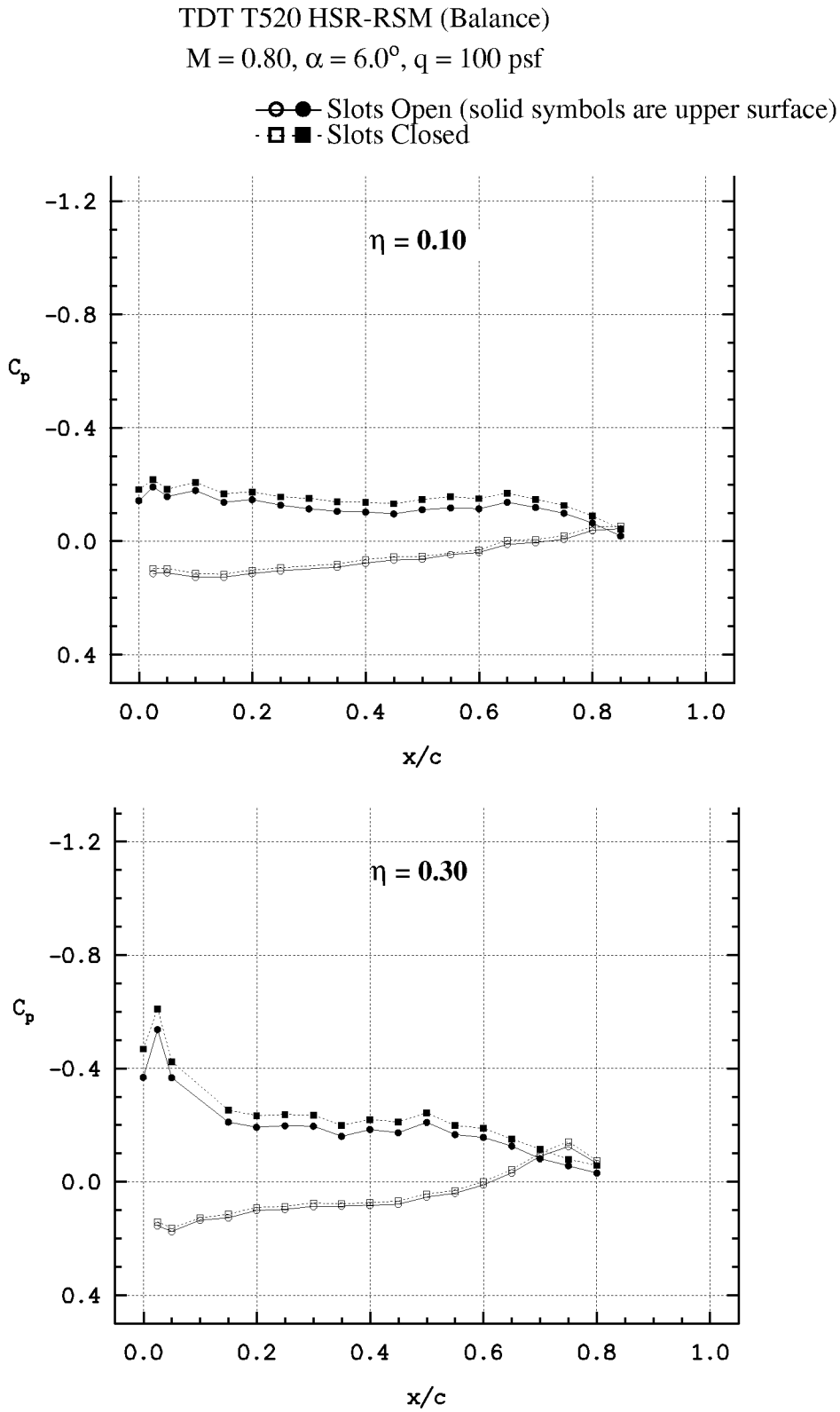

Figure 19. Comparison of wind tunnel wall slots open and closed pressure data at M=0.8, α=6.0°.

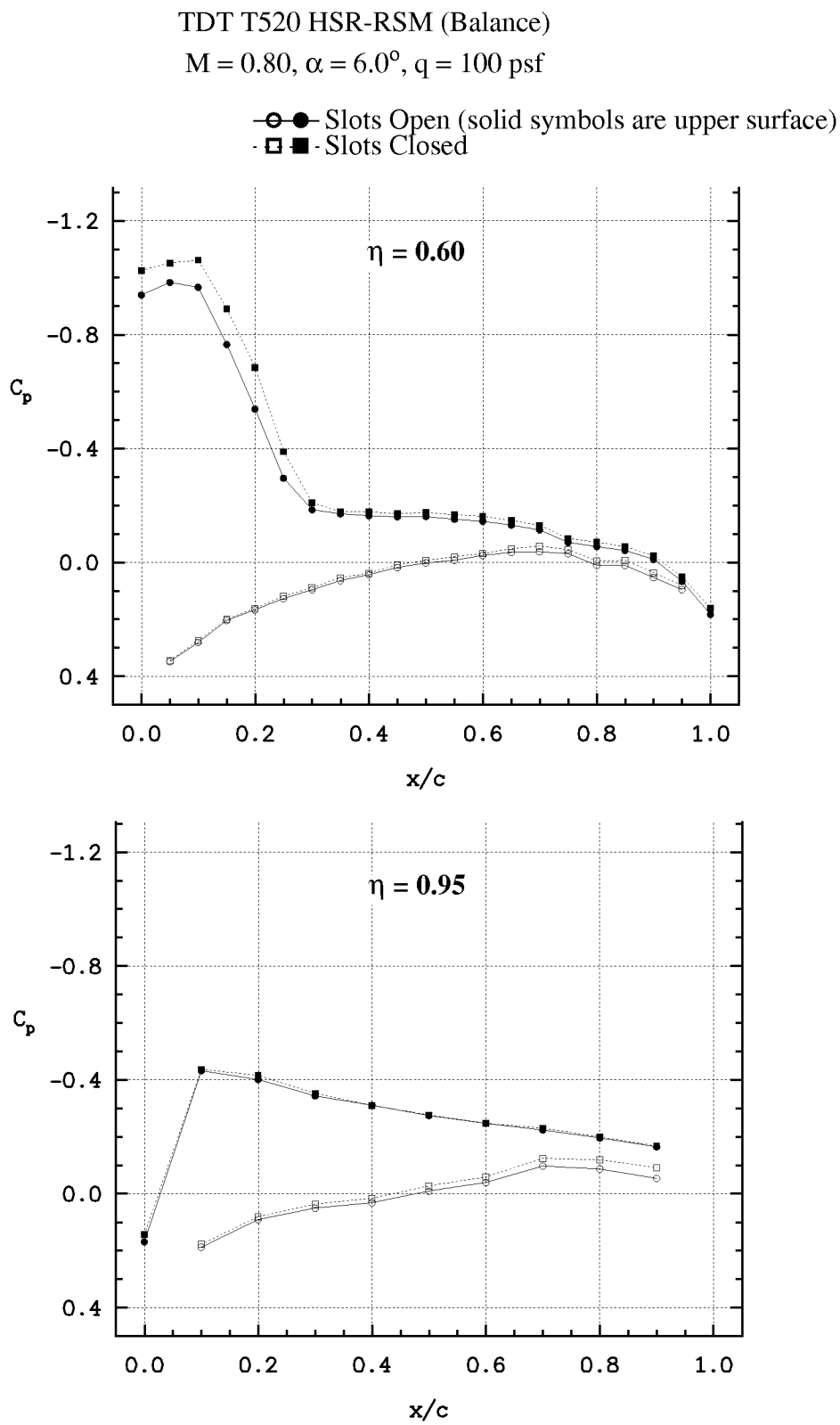

Figure 19(Continued). Comparison of wind tunnel wall slots open and closed pressure data at M=0.8, α=6.0°.

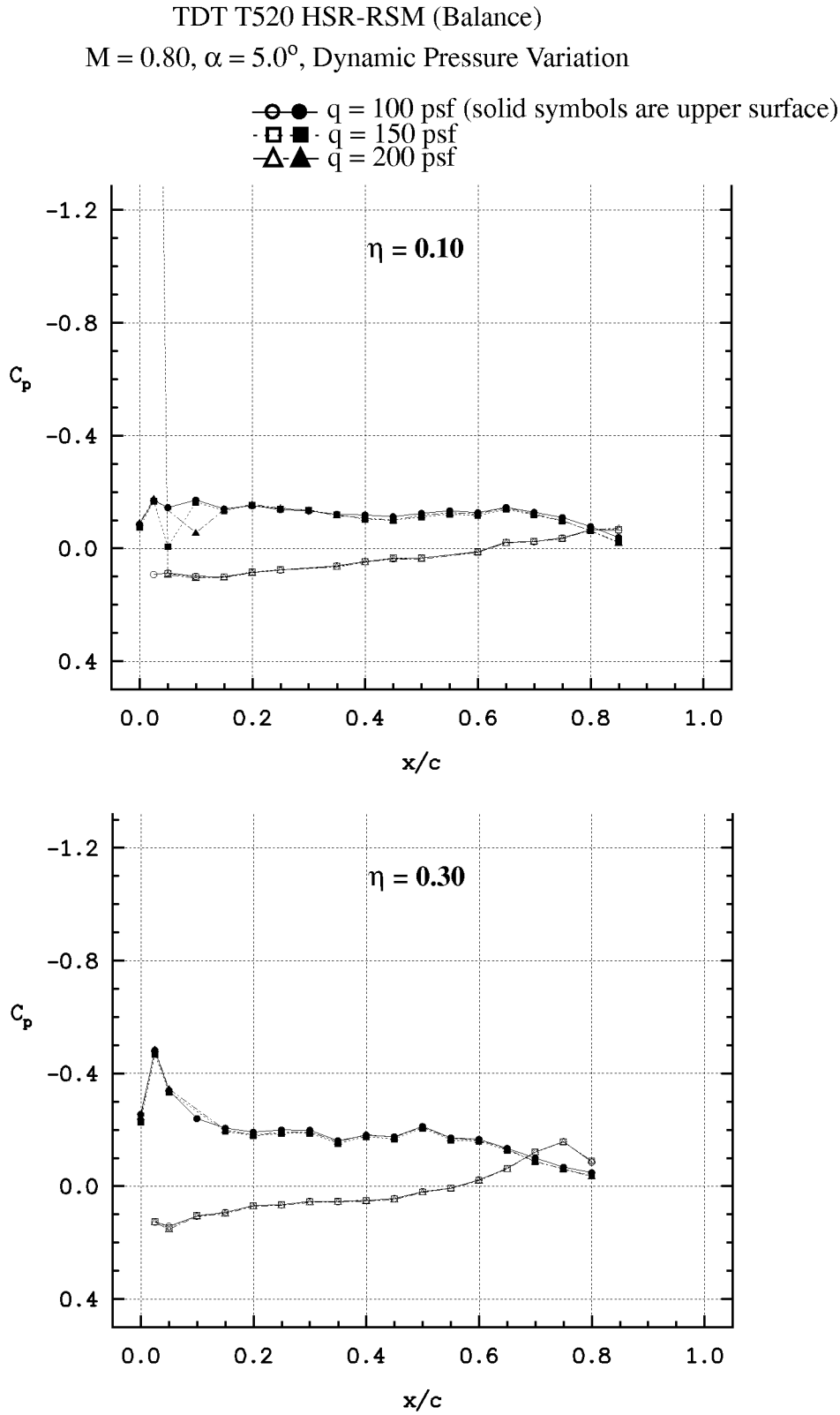

Figure 20. Comparison of pressure data as a function of dynamic pressure.

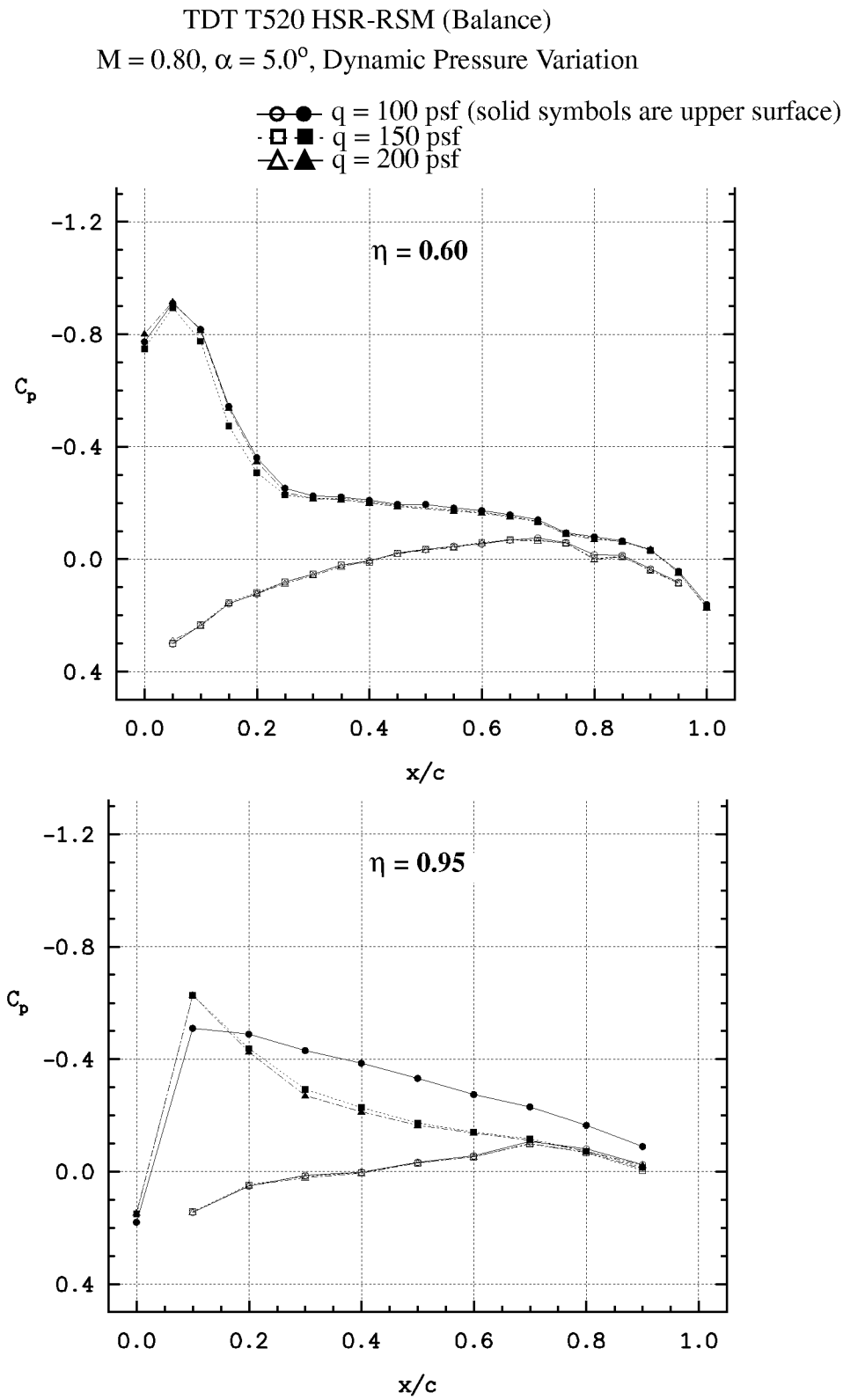

Figure 20(Continued). Comparison of pressure data as a function of dynamic pressure.

Comparison of Clean-Wing and Nacelles-On Pressure Data

Figure 21 compares the pressure distribution data at Mach 0.95 and 5 degrees angle-of-attack for the clean-wing and nacelles-on configurations. These data correspond to the previously presented loads data of Figure 10. Once again, we see trends in the pressure data which do not correlate with conventional wisdom for this type of configuration change. At the inboard stations near the nacelles, we see a moderate change in the pressure distribution on the aft portion of the wing. The largest change in the pressures is on the lower surface, which is to be expected since this is where the nacelles are mounted. What is somewhat unexpected is the significant impact that the nacelles have on the outboard span station pressures. At 60% span, the nacelles impact virtually the entire pressure distribution on the lower surface of the wing. They also have a significant effect on the upper surface pressures from 40% chord aft. The nacelles are mounted at approximately 17% and 40% span, so it is expected that they will have some effect on the pressures at 60% span. However, it is interesting to note the magnitude of the effect. At 95% span, the differences between the pressure distributions for the two configurations seem to be further magnified. Again, the lower surface of the wing is significantly affected, but the pressure distribution on virtually the entire upper surface is also markedly different from that of the clean-wing configuration. As with the dynamic pressure data, the clean-wing versus nacelle data require more analysis before meaningful conclusions can be drawn. If the trends displayed in this report are indicative of the data at other flight conditions, prediction of these trends will provide an interesting challenge for computational methods.

Impact of Flap Deflection on Pressure Distribution

As a final analysis of the wing pressures, we will look at how Mach number affects the clean-wing pressure distribution with the flaps deflected. Recalling the discussion of Figure 15, we noted the significant variation of the lift due to flap deflection with Mach number. It was speculated that the flap was interacting with a shock wave that resulted in reduced control surface effectiveness as Mach number is increased. The pressure data of Figure 22 support this assertion. This figure separately plots the upper and lower surface pressure distributions for each span station at 2 degrees angle-of-attack and 4 degrees flap deflection for 0.95, 0.98, and 1.10 Mach number. Looking at the 10% and 30% span stations, it is difficult to see how the Mach number affects the flow on the flap since there are no pressure orifices on the flap itself. Examination of the pressure distributions ahead of the flap does not indicate any significant alteration of the flow as Mach number is increased. At the 60% span station however, we see the formation of a shock at approximately 90% chord on the upper surface which progressively travels aft as Mach number is increased. It can be inferred from this pressure distribution that the flow on the inboard portion of the wing behaves in a similar fashion. The lower surface pressures at 60% span provide further reinforcement for this hypothesis.

This is one area where computational methods can be used in conjunction with the experimental data to help fill in parts of the picture that are missing due to testing constraints, instrumentation limitations, etc. Thus the value of these data go well beyond simple CFD code correlation. They provide insight to strategies for combining experimental programs with computational methods to understand complicated flow phenomena without the expense of a fully instrumented model. Demonstration of such a capability would allow us to build confidence in CFD as a tool which can be used in concert with experimental data to accurately predict and understand the physical characteristics of the flow about complex vehicles. This is an especially important concept for

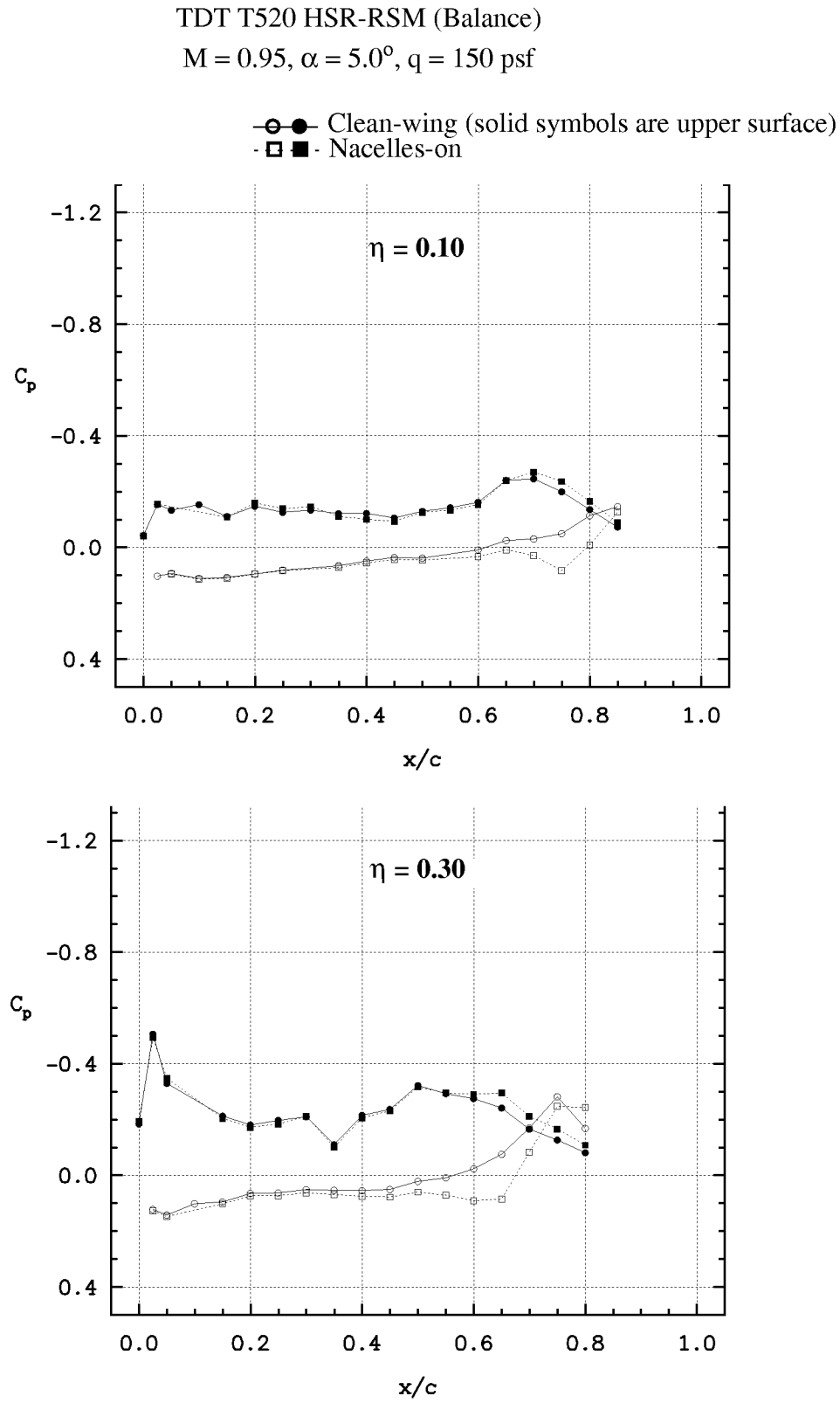

Figure 21. Comparison of clean-wing and nacelles-on pressure data at M=0.95, α=5.0°.

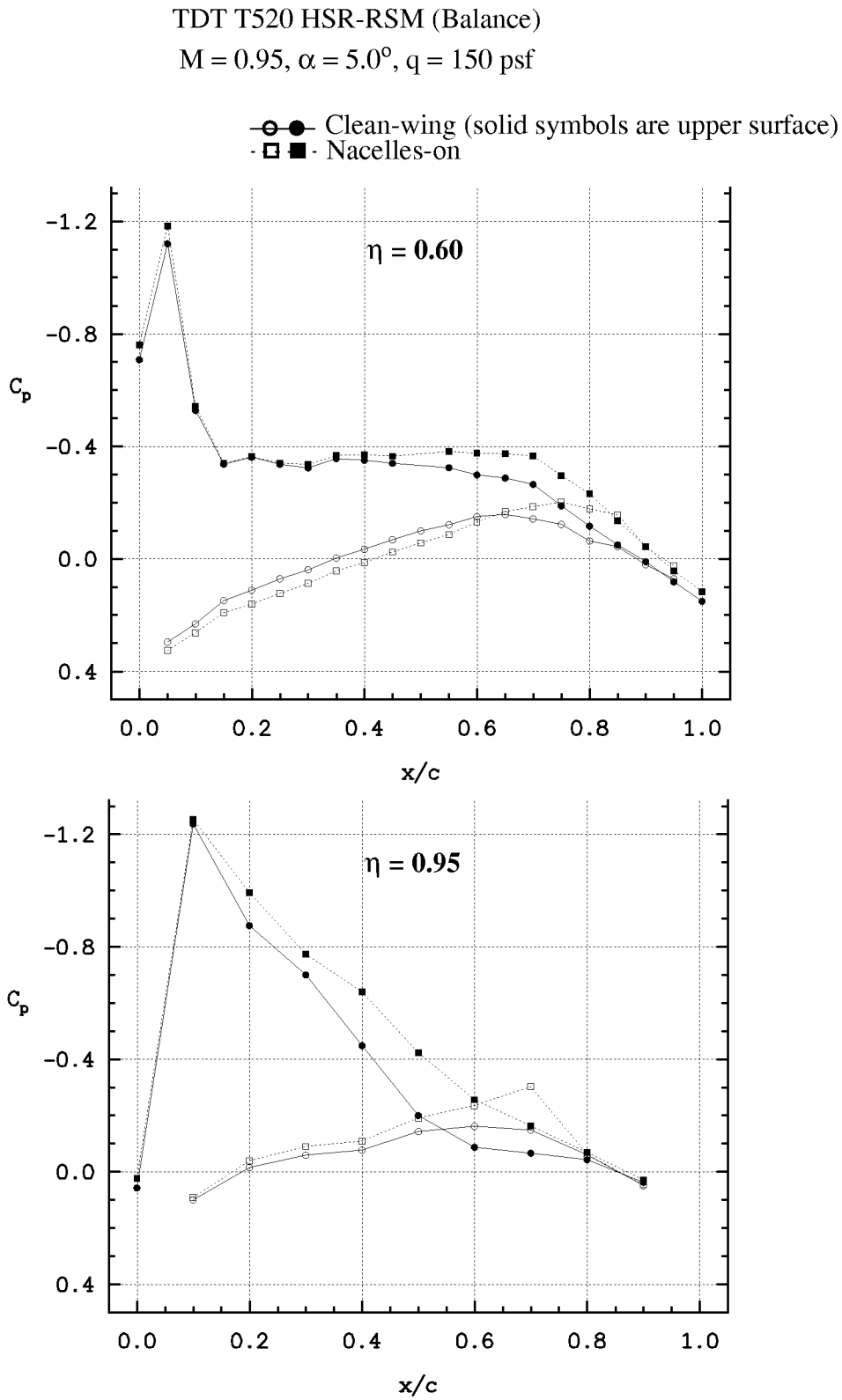

Figure 21(Continued). Comparison of clean-wing and nacelles-on pressure data at M=0.95, α=5.0°.

TDT T520 HSR-RSM (Balance)
$\alpha = 2.0^o$, $\delta_f = 4.0^o$, q = 150 psf
Upper Surface Pressure Distributions

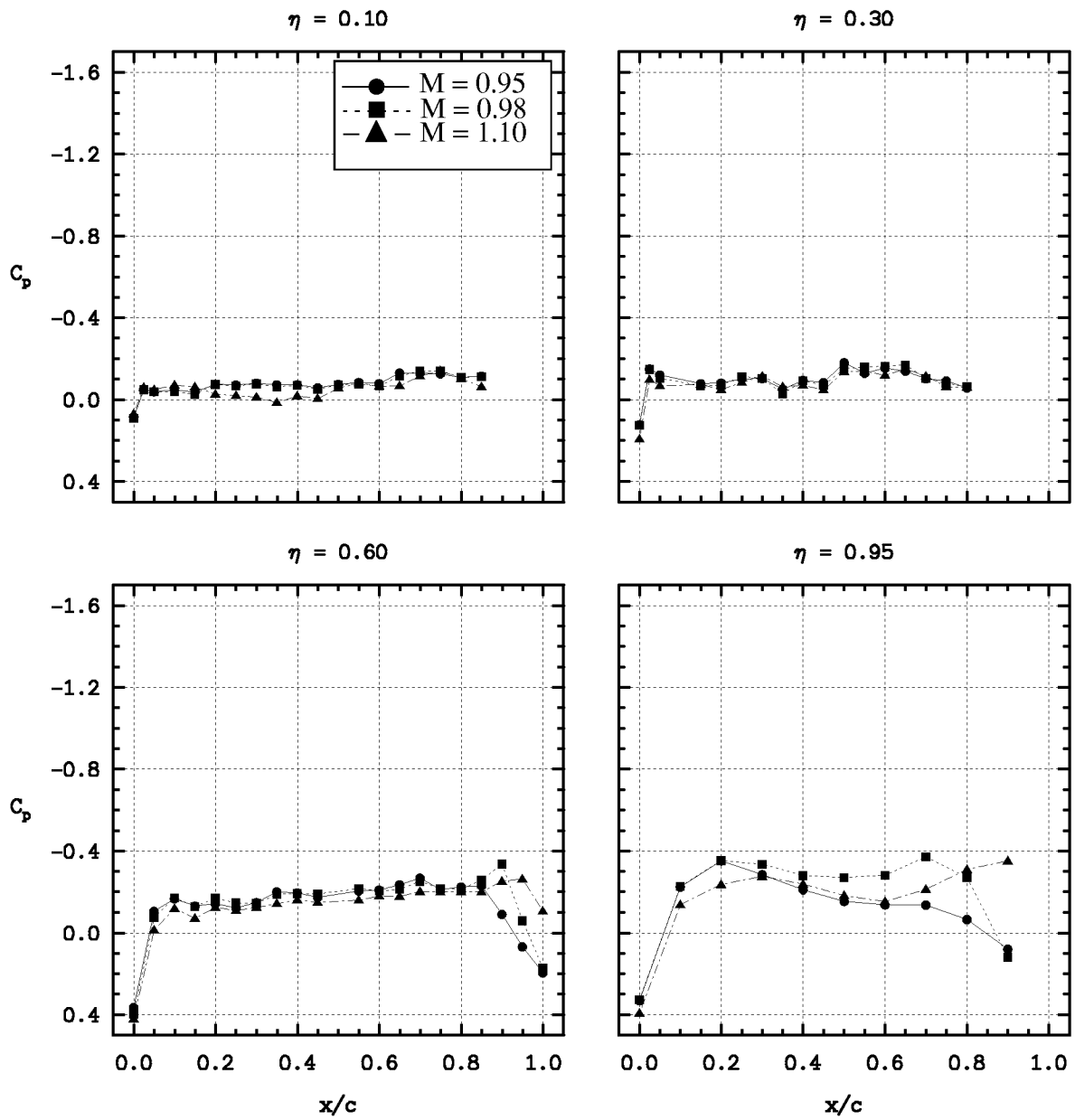

Figure 22. Pressure distribution variation with Mach number for clean-wing with deflected flap.

TDT T520 HSR-RSM (Balance)
$\alpha = 2.0^o$, $\delta_f = 4.0^o$, q = 150 psf
Lower Surface Pressure Distributions

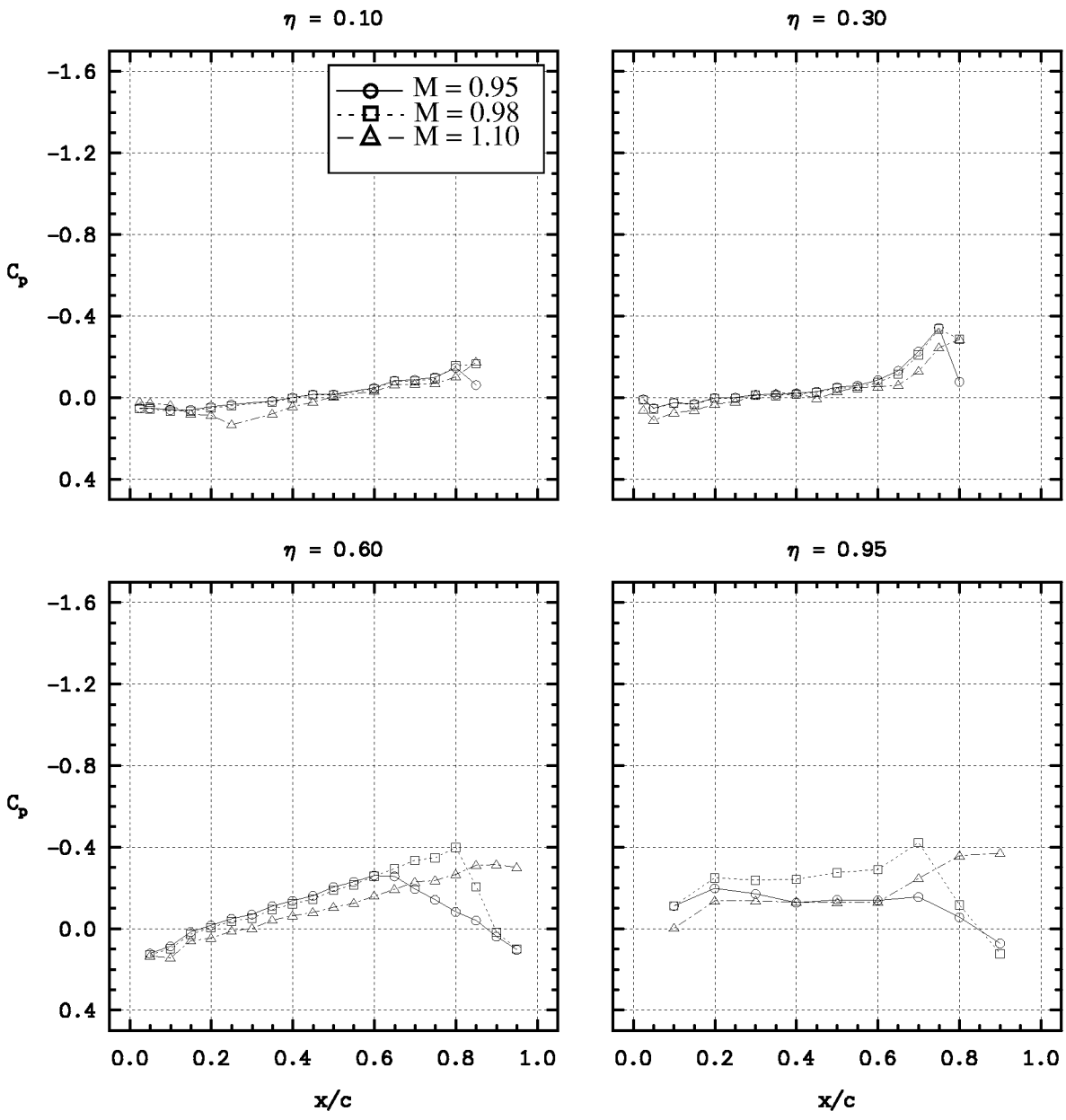

Figure 22(Continued). Pressure distribution variation with Mach number for clean-wing with deflected flap.

unsteady testing since it is often very difficult to acquire accurate unsteady data in a quantity sufficient for detailed aerodynamic and structural analysis.

CONCLUSION

Transonic Dynamics Tunnel Test 520 of the HSR Rigid Semispan Model has provided a large quantity of high quality force and pressure data for use in correlation with computational fluid dynamics methods. Data were collected for a wide range of model configurations and test conditions, and the primary objectives of the test have been met. From a CFD code correlation standpoint, detailed wing and fuselage pressure data were acquired which can be compared directly with pressure distributions computed by CFD analyses. Loads data from a five component force balance were acquired for each set of pressure distributions so that integrated CFD loads can be compared with accurate experimental loads. The test setup was careful to isolate the wing loads from the fuselage load so that the highly nonlinear flow about the fuselage/wind tunnel wall combination would not complicate the process of comparing the experimental loads with the more idealistic loads computed by CFD methods. Even with these precautions, one should be careful to consider the influence of the wind tunnel walls and blockage when comparing these data with analytical results. In particular, the build up of the boundary layer on the sidewall of the tunnel should be examined and an assessment of its impact on the experimental data should be formulated. Experiments with the TDT east wall slots open and closed show that the aerodynamic data are sensitive to the conditions along this wall. Since the model was not tested with a splitter plate, the boundary layer along this wall could have had a significant impact on the aerodynamic data.

Each data point acquired in the TDT represents a unique set of flow conditions and configuration, but the loads data were not reduced and organized into typical aerodynamic polar form during the course of the test. This task was accomplished post test. The lift and moment curves were approximated using a linear least squares fit, and the drag as a function of lift was fit using a second order curve. Parameters such as lift curve slope, minimum drag, etc. can be extracted from these curve fits. Higher order fits of the data were also investigated, but these fits produced less consistent data when certain parameters such as lift curve slope were correlated against Mach number. All of the loads data have been tabulated, plotted, written to a CD-ROM volume and distributed to the HSR industry partners.

Unsteady wing pressure data and steady fuselage pressure data were acquired, reduced, written in tabular form and plotted on-line during the test. The tabular pressure data and plots have also been accumulated into a CD-ROM volume and distributed. The tabulated data were written in an ASCII formatted channel statistics file which can be easily read and post processed. The steady fuselage pressure data are organized into rows of pressures along constant fuselage sections, while the wing pressures are organized into chordwise rows at four constant span stations. In addition to time averaged wing pressures, unsteady pressure measurements were also made for cases where the trailing edge control surface was oscillated. ASCII files of these time histories have been included in the previously delivered data package.

In this report, the data were examined for its overall consistency and adherence to established aerodynamic trends. The variation of the data with angle-of-attack and Mach number has been shown to be reasonable. The lift data is linear with angle-of-attack at low to moderate lift coefficients as are the pitching moment data. The drag is nearly quadratic with lift. Similar

aerodynamic characteristics are observed with control surface deflection. The variation of the angle-of-attack polar data with Mach number produced no major surprises, but the flap deflection data show a wide range of control surface effectiveness with variation of Mach number. Speculation that this is an interaction between shock waves and the control surface was shown to be supported by the wing pressure data. The variation of the data with dynamic pressure showed no significant static aeroelastic issues, but a localized difference in the 100 psf data near the wing tip warrants further investigation. Though repeatability was never specifically evaluated, the dynamic pressure comparison implicitly addresses this issue. Except for the 95% span upper surface location, where there is an obvious flow anomaly in the 100 psf data, the pressure data for the three dynamic pressures are very consistent. These three dynamic pressures were tested with several runs and tunnel entries between corresponding points, and they exhibit outstanding repeatability.

There were only two experiment configuration changes performed during this test. The TDT east wall slots were tested in an open and closed condition, and the wing was tested in a clean-wing and nacelles-on configuration. Closing the wall slots was shown to have a significant impact on the aerodynamic loads. The pressure distributions for the slots-open and -closed data showed that the upper surface flow was especially sensitive to the status of the slots at positive lift conditions. It is speculated, but has not been confirmed, that the lower surface pressures would be more sensitive to slot configuration at negative lift conditions. The slots affect the wing pressures to at least 60% span. Verifying these results computationally will be very difficult, and further testing of semispan models with the east wall slots open and closed should probably be performed before making general conclusions about their importance.

The addition of the flow-through nacelles to the inboard trailing edge of the wing is shown to have a significant impact on the flow over the entire wing. In the general vicinity of the nacelles, the changes to the flow appear to be localized in nature, with the pressure distributions ahead of the nacelles showing only small response to their presence. However, the pressure distribution on the outboard sections of the wing appear to be heavily influenced by the nacelles. It will be interesting to see if computational methods produce these same trends.

The analyses presented in this report were chosen so as to illustrate and verify the quality of the data acquired during this test. In the course of this presentation we have uncovered some thought-provoking issues with the data that deserve more attention than what could be afforded in this cursory examination. These data can and should be used in conjunction with computational methods not only to verify the computations, but also to gather insight into some of the phenomena described herein. We feel that the data taken during this test are of sufficient quality and resolution to be useful to a wide range of both steady and unsteady computational methods verification studies. In addition, there is great potential for computational methods to be used to assist in resolving and providing physical insight into many of the somewhat puzzling aerodynamic characteristics observed during this test.

REPORT DOCUMENTATION PAGE

Form Approved
OMB No. 07704-0188

Public reporting burden for this collection of information is estimated to average 1 hour per response, including the time for reviewing instructions, searching existing data sources, gathering and maintaining the data needed, and completing and reviewing the collection of information. Send comments regarding this burden estimate or any other aspect of this collection of information, including suggestions for reducing this burden, to Washington Headquarters Services, Directorate for Information Operations and Reports, 1215 Jefferson Davis Highway, Suite 1204, Arlington, VA 22202-4302, and to the Office of Management and Budget, Paperwork Reduction Project (0704-0188), Washington, DC 20503.

1. AGENCY USE ONLY *(Leave blank)*

2. REPORT DATE
September 1999

3. REPORT TYPE AND DATES COVERED
Contractor Report

4. TITLE AND SUBTITLE
Transonic Dynamics Tunnel Force and Pressure Data Acquired on the HSR Rigid Semispan Model

5. FUNDING NUMBERS
537-06-36
NAS1-96014

6. AUTHOR(S)
David M. Schuster and Russ D. Rausch

7. PERFORMING ORGANIZATION NAME(S) AND ADDRESS(ES)
Lockheed Martin Engineering and Sciences
Mail Stop 371
Hampton, VA 23681-2199

8. PERFORMING ORGANIZATION REPORT NUMBER

9. SPONSORING/MONITORING AGENCY NAME(S) AND ADDRESS(ES)
National Aeronautics and Space Administration
Langley Research Center
Hampton, VA 23681-2199

10. SPONSORING/MONITORING AGENCY REPORT NUMBER
NASA/CR-1999-209555

11. SUPPLEMENTARY NOTES
Langley Technical Monitor: Thomas E. Noll

12a. DISTRIBUTION/AVAILABILITY STATEMENT
Unclassified–Unlimited
Subject Category 02 Distribution: Nonstandard
Availability: NASA CASI (301) 621-0390

12b. DISTRIBUTION CODE

13. ABSTRACT *(Maximum 200 words)*
This report describes the aerodynamic data acquired on the High Speed Research Rigid Semispan Model (HSR-RSM) during NASA Langley Transonic Dynamics Tunnel (TDT) Test 520 conducted from 18 March to 4 April, 1996. The purpose of this test was to assess the aerodynamic character of a rigid high speed civil transport wing. The wing was fitted with a single trailing edge control surface which was both steadily deflected and oscillated during the test to investigate the response of the aerodynamic data to steady and unsteady control motion. Angle-of-attack and control surface deflection polars at subsonic, transonic and low-supersonic Mach numbers were obtained in the tunnel's heavy gas configuration. Unsteady pressure and steady loads data were acquired on the wing, while steady pressures were measured on the fuselage. These data were reduced using a variety of methods, programs and computer systems. The reduced data was ultimately compiled onto a CD-ROM volume which was distributed to HSR industry team members in July, 1996. This report documents the methods used to acquire and reduce the data, and provides an assessment of the quality, repeatability, and overall character of the aerodynamic data measured during this test.

14. SUBJECT TERMS
Aerodynamic characteristics; Supersonic transport; Aircraft stability and control; Aeroelasticity

15. NUMBER OF PAGES
50

16. PRICE CODE
A03

17. SECURITY CLASSIFICATION OF REPORT
Unclassified

18. SECURITY CLASSIFICATION OF THIS PAGE
Unclassified

19. SECURITY CLASSIFICATION OF ABSTRACT
Unclassified

20. LIMITATION OF ABSTRACT
UL